Drug Delivery and Translational Research
https://doi.org/10.1007/s13346-020-00822-4

ORIGINAL ARTICLE

Phospholipid complex-loaded self-assembled phytosomal soft nanoparticles: evidence of enhanced solubility, dissolution rate, ex vivo permeability, oral bioavailability, and antioxidant potential of mangiferin

Darshan R. Telange[1] · Nazish K. Sohail[2] · Atul T. Hemke[2] · Prashant S. Kharkar[3] · Anil M. Pethe[4]

Abstract

In this study, self-assembled phytosomal soft nanoparticles encapsulated with phospholipid complex (MPLC SNPs) using a combination of solvent evaporation and nanoprecipitation method were developed to enhance the biopharmaceutical and antioxidant potential of MGN. The mangiferin-Phospholipon® 90H complex (MPLC) was produced by the solvent evaporation method and optimized using central composite design (CCD). The optimized MPLC was converted into MPLC SNPs using the nanoprecipitation method. The physicochemical and functional characterization of MPLC and MPLC SNPs was carried out by differential scanning calorimetry (DSC), thermogravimetric analysis (TGA), Fourier-transform infrared spectroscopy (FT-IR), powder X-ray diffractometer (PXRD), proton nuclear magnetic resonance (^{1}H-NMR), solubility, in vitro dissolution, oral bioavailability, and in vivo antioxidant studies. A CCD formed stable MPLC with the optimal values of 1:1.76, 50.55 °C, and 2.02 h, respectively. Characterization studies supported the formation of a complex. MPLC and MPLC SNPs both enhanced the aqueous solubility (~ 32-fold and ~ 39-fold), dissolution rate around ~ 98% via biphasic release pattern, and permeation rate of ~ 97%, respectively, compared with MGN and MGN SNPs. Liver function tests and in vivo antioxidant studies exhibited that MPLC SNPs significantly preserved the CCl_4-intoxicated liver marker and antioxidant marker enzymes, compared with MGN SNPs. The oral bioavailability of MPLC SNPs was increased appreciably up to ~ 10-fold by increasing the main pharmacokinetic parameters such as C_{max}, T_{max}, and AUC. Thus, MPLC SNPs could be engaged as a nanovesicle delivery system for improving the biopharmaceutical and antioxidant potential of MGN.

Keywords Mangiferin · Solubility · In vitro dissolution rate · Oral bioavailability and in vivo antioxidant potential

Introduction

Mangiferin (MGN), a xanthonoid predominantly found in the leaves, bark, fruits, and root bark of plants such as *Mangifera indica* (Family: Anacardiaceae) and others, is a super-antioxidant [1–6]. Following oral administration, it offers a score of health benefits such as antioxidants [7], blood lipid-lowering agents [8], anti-proliferative [9], skeletal muscle contractile [10], and brain oxygenation [11]. Recently Imran et al. [4] have extensively reviewed the potential of MGN in managing lifestyle-related disorders. Enormous literature reports are available demonstrating the utility of MGN in a variety of diseases and disorders. MGN is being consistently explored in life sciences, particularly during the last decade or so, as seen from the number of published papers. Yang et al. reported the protective effect of MGN on cerebral ischemia-reperfusion

✉ Darshan R. Telange
telange.darshan@gmail.com

[1] Rajarshi Shahu College of Pharmacy, Malvihir, Botha Road, Buldhana, Maharashtra, India

[2] Smt. Kishoritai Bhoyar College of Pharmacy, Nagpur, Maharashtra, India

[3] Shobhaben Pratapbhai Patel School of Pharmacy and Technology Management, SVKM's NMIMS (Deemed to be University), V.L.Mehta Road, Vile Parle (W), Mumbai, Maharashtra, India

[4] School of Pharmacy and Technology Management, SVKM's NMIMS (Deemed to be University), Polepally SEZ, Jadcherla, Mahbubnagar, Hyderabad, Telangana, India

Published online: 21 July 2020

injury via enhancing the activation of the Nrf2/HO-1 pathway [12]. Bhatt et al. reported the cardioprotective activity of MGN against cyclophosphamide-induced cardiotoxicity via enhancing lipid profile, antioxidant level, and electrocardiographic parameters [13]. Szandurk et al. investigated the protective effect of MGN on trinitrobenzene sulfonic acid-induced colitis in rats and found that MGN at 30 and 100 mg/kg improved the colitis condition in rats by reducing TNF-α and IL-17 concentration [14]. Sahu et al. investigated the defensive role of MGN against cisplatin-induced nephrotoxicity. Results demonstrated that MGN at a dose of 20 and 40 mg/kg appreciably reversed the renal function [15]. Despite the potential offered by MGN as a medicinal agent and a nutraceutical, its benefits are strongly confined by its nearly undesirable biopharmaceutical and pharmacokinetic properties such as low aqueous solubility (0.1 to 0.3 mg/mL), deprived lipophilicity (logP 0.56), limited and variable oral bioavailability (1.5 to 5%), rapid phase II metabolism (glucuronidation), shorter half-life ($t_{1/2}$) (1.71 h), and fast clearance from the human body [16–20]. It is categorized as the Biopharmaceutical Classification System (BCS) class IV drug. The presence of four phenolic -OH groups contribute significantly to its extensive glucuronidation, following oral administration [21], compromising its oral bioavailability and subsequent therapeutic benefits.

A significant number of formulation strategies have been explored so far to overcome the above biopharmaceutical challenges associated with MGN. These attempts include β-cyclodextrin (β-CD) inclusion complexation [22], salt formation [23], phospholipid complexation [17, 18], nanostructured lipid carrier system [24], and spray-dried formulation [25]. A detailed analysis of these formulation trials demonstrated variable and limited success. Moreover, the phospholipid complexation work of Khurana et al. [17, 18] has shown the limited improvements in solubility (25-fold only) and dissolution studies without investigating optimization, entrapment efficiency, oral bioavailability, and in vivo antioxidant activity of complex and/or nanostructured lipid carriers (NLCs). Additionally, the author has used Phospholipon® 90G, for the preparation of phospholipid complex even though it exhibits low solubility for MGN. Phospholipon® 90G is reported to form strong aggregates and agglomeration with drug and/or bioactive which, in turn, results to the decrease in the solubility and dissolution performance of drug and/or bioactive [26]. With the consideration of this, we, therefore, used a novel dual-formulation approach to overcoming the observed limitations of the previously reported formulations and/or drug delivery systems (DDS), by designing and developing an alternate formulation or DDS addressing the existing pain-in-the-brain biopharmaceutical issues associated with MGN.

Of the several strategies for enhancing the aqueous solubility of poorly water-soluble drugs in general and BCS class IV drugs in particular, complexation with phospholipids presents a unique and appropriate strategy. Previously, this modality has been used successfully for improving the poor aqueous solubility, in vitro release rate, and most importantly, the oral bioavailability of plant-based bioactive such as daidzein [27], salvianolic acid B [28], chlorogenic acid [19], kaempferol, and apigenin [29, 30]. Moreover, a phospholipid-based system, i.e., formulation, offers several benefits such as ease of preparation, high drug loading capacity, and long-term stability, to name a few. Furthermore, the utilized Phospholipon® 90H and nanoprecipitation method in the current study convert the system into soft nanoparticles with significant improvement in solubility, dissolution, absorption, and finally oral bioavailability of MGN.

Self-assembled phytosomal soft nanoparticles (SNPs) are lipid-compatible molecular aggregates that form a micelle-like spherical structure. This delivery system has created significant interest among researchers due to several benefits such as controlled release, maximization of therapeutic efficacy, minimization of side effects, gastric protection from luminal enzymes, ease of fabrication, drug stability, and, most importantly, transportation of drugs across the biological barriers. SNPs are consisting of bioactive and phospholipids. Phospholipids are compound lipids, which act as a major part of the biomembrane as well as a precursor in the formation of platelet activation factor, arachidonic acid, and secondary messengers used in the process of signal transduction [31–33]. As a part of the biomembrane, phospholipids demonstrate good biocompatibility and, thus, serve as excellent drug delivery carriers in the transportation of drugs across the biological barrier [34]. The presence of positive and negative charges in the phospholipid compound makes it amphiphilic, which shows lipid as well as water solubility to a greater extent [35, 36]. The presence of hydroxyl group (-OH) of phospholipids can make successful interactions with active hydrogen part of any lipophilic drug via esterification process, leading to produce an amphiphilic compound which further can improve the therapeutic activity of drug molecule via facilitating its transportation across lipid-rich biomembrane [37]. Moreover, this physicochemical property of phospholipids is also employed in the formation of a complex with bioactive through polar and hydrogen bonding interactions [38–40]. Earlier literature has shown that phospholipid complex improved the aqueous solubility, permeability, stability, and site specificity, thereby enhancing the oral bioavailability and efficacy and reducing the toxic side effects of hydrophobic drugs [41]. Additionally, the formation of self-assembled amphiphilic structure [42], biocompatibility [43], emulsifying [44], and wetting characteristics [42] of phospholipids provide a base material for the preparation of nanoparticles' drug delivery system. Nanoprecipitation technology is a nanoparticle preparation technique, in which the SNPs are prepared by diffusing the organic phase containing complex into the continuous water phase leading to the formation of o/w suspension. Further

rapid diffusion leads to a decreased interfacial tension and evaporation of the organic solvent, resulting in the formation of self-assembled phytosomal SNPs as nanodroplets loaded with phospholipid complex. Formations of SNPs using this technology can result in amphiphilic nanoparticles which can entrap bioactive and phospholipid complex to a greater extent and facilitate the transfer of complex loaded into SNPs from water-soluble location to the lipid-soluble location of cell membrane for exhibiting high drug efficacy [45]. Therefore, self-assembled phytosomal SNPs are considered to be the promising dual-formulation technology for improving the biopharmaceutical attributes of many bioactive. Many pharmaceutical scientists devised a combined formulation strategy involving two or more carriers such as polymer gel [46], phospholipid complex loaded in microspheres [47], and phospholipid complex-loaded matrix film [48]. These unique formulations exhibited significant improvement in the biopharmaceutical profile of the loaded drug or phytoconstituents. Previously, it was demonstrated that a noteworthy enhancement of biopharmaceutical properties of drugs relied upon the successful incorporation of the phospholipid complex into the nanosystems [49–51]. To the best of our knowledge, such a novel formulation strategy has not been reported so far in the literature.

In the present study, we report a systematic and comprehensive study of novel dual-formulation strategy for improving the biopharmaceutical profile of a super-antioxidant MGN, with a potential impact on its bioavailability and therapeutic utility. The formulations were optimized using the design of experiments (DoE) methodology, followed by the physicochemical and biopharmaceutical characterization (particle size, zeta potential, detailed thermal, spectroscopic, powder X-ray diffraction, solubility, in vitro dissolution studies, etc.). Finally, the optimized formulations were functionally evaluated for their antioxidant potential in vivo in carbon tetrachloride (CCl_4)-intoxicated albino rat model.

Materials and methods

Mangiferin (HPLC purity > 99%) was obtained from Sisco Research Laboratories Pvt. Ltd. Mumbai, India. Phospholipon® 90H was obtained from Lipoid GmbH, Ludwigshafen, Germany. Carbon tetrachloride, chloroform, ethylenediaminetetraacetic acid (EDTA), 5,5′-dithiobis-2-nitro benzoic acid (DTNB), sodium chloride, sodium lauryl sulfate, and Tween® 20 were obtained from Loba Chemicals Pvt. Ltd., Mumbai, India. n-Hexane, 1-octanol, m-phosphoric acid, thiobarbituric acid, and trichloroacetic acid were obtained from Sigma Chemicals, Sigma-Aldrich Corporation, St. Louis, MO. All other chemicals were of analytical grade unless otherwise mentioned.

Formulation of mangiferin-phospholipid complex (MPLC)

A well-established solvent evaporation method described previously by Zhang et al. [47] was used for the preparation of MPLC. Briefly, MGN (MW, 422.33 g/mol) and Phospholipon® 90H (MW, 790 g/mol) were individually weighed in molar ratios 1:0.51, 1:1.02, 1:1.76, 1:2.5, or 1:3 and then transferred to a clean 100-mL round-bottom flask. The contents of the flask were dissolved in absolute EtOH (20 mL) and stirred well. The solution was heated under controlled conditions 40.14/44.2/50.15/56.1/60.15 °C on water bath (DSY-2-2, Aiqixia Apparatus Center, China) for 1.01/1.42/2.01/2.6 or 3.0 h, respectively. The solvent was evaporated and the residue was mixed with n-hexane (10 mL), leading to precipitation of MPLC. Further subsequent filtration and drying under vacuum at 40 °C for 12 h yielded the product, which was stored at room temperature (RT) in an amber-colored glass vial, previously flushed with nitrogen (N_2), until further use.

The rationale for selecting independent, dependent variables and their ranges

The independent, dependent variables and their ranges were selected based on preliminary experiments, supporting literature, and central composite design. A phytosome (drug-phospholipid complex) is a molecular aggregate of the drug-phospholipid complex. Therefore, MPLC was prepared using the same procedure as mentioned above [35] and explored for the selection of independent, dependent variables and their ranges. After the selection of variables and their range, the MPLC was optimized at five levels using the above-mentioned design.

Central composite design (CCD)

The MPLC formulation was optimized using CCD (Design-Expert®, Version 10.0.4.0, Stat-Ease Inc., Minneapolis, MN, USA) to obtain precise information on the formulation/process variables with a reasonably lower number of experimental trials. In the present study, we have chosen three independent variables, namely, MGN/phospholipids ratio (X_1, w:w), reaction temperature (X_2,°C), and reaction time (X_3, h), respectively. The chosen variables were investigated at five levels and were coded as − 1.73, − 1, 0, + 1, and + 1.73. The extent of the complexation rate or yield (%) was chosen as a dependent (response) variable. The detailed analysis led to 20 possible runs. These formulations were prepared and assessed one by one for the dependent variable, i.e., yield (%). Upon fitting the data, a statistical model, i.e., a polynomial equation along with a desirability plot, was obtained. The

model (Eq. 1) listed the coefficients of the variables and the quadratic and interaction terms having a significant influence on the dependent variable:

$$Y = b_0 + b_1X_1 + b_2X_2 + b_3X_3 + b_{11}X_1^2 + b_{22}X_2^2 + b_{33}X_3^2 + b_{12}X_1X_2 + b_{23}X_2X_3 + b_{13}X_1X_3 \quad (1)$$

where Y is the dependent variable, b_o, the intercept of the arithmetic average of 20 experimental trials, and b_1 to b_{13} represents the calculated coefficients of (X_i, $i = X_1, X_2,$ *and* X_3). X_1, X_2, and X_3 are the main effects. The interaction terms X_1X_2, X_2X_3, and X_1X_3 are the combined effects of the independent variables, while polynomial terms X_1^2, X_2^2, and X_3^2 signify the nonlinear dependency of the response variable on the inputs. Table 1 lists the details of the experimental trials along with the coded and real values of both, the independent and dependent variables. The CCD and the experimental trials with calculated values of yield (%) are given in Table 2.

Estimation of the extent of MGN complexation in prepared MPLC (% yield)

The extent of MGN complexation in MPLC formulations was determined using UV-visible spectroscopy [52]. Briefly, MPLC (equivalent to ~ 50 mg of MGN) was transferred to a beaker, followed by mixing with chloroform (5 mL). In the resulting dispersion, the MPLC and Phospholipon® 90H were dissolved completely while MGN precipitated out. The insoluble MGN was allowed to settle and the dispersion is filtered using Whatman® quantitative filter paper (ashless, Grade 41, Sigma-Aldrich Corporation, St. Louis, MO), dried, dissolved in methanol, suitably diluted, and assayed at the detection wavelength (~ 259 nm) using a UV-visible spectrophotometer (Model: V-630, JASCO International Co., Ltd., Tokyo, Japan). The extent of the complexation of MGN with phospholipids was calculated by Eq. 2:

$$Extent\ of\ complexation\ (\%) = \left(c_t - c_f\right)/c_t \times 100 \quad (2)$$

where c_t is the theoretical concentration of MGN in MPLC and c_f is the observed concentration of MGN in the filtrate.

Table 2 Central composite design experimental trial formulation batches with obtained yield values (%, *w*/w)

Experimental trials	X_1	X_2	X_3	Extent of complexation, or yield* (%, w/w)
1	−1	+1	−1	59.20 ± 0.11
2	+1	−1	−1	84.02 ± 0.09
3	−1	−1	+1	78.30 ± 0.43
4	+1	+1	−1	82.10 ± 0.26
5	0	0	0	91.30 ± 0.56
6	+1.73	0	0	87.24 ± 0.51
7	0	0	0	90.16 ± 0.63
8	+1	+1	+1	86.26 ± 0.17
9	0	0	0	88.12 ± 0.24
10	0	0	+1.73	97.71 ± 0.33
11	−1	−1	−1	72.38 ± 0.40
12	0	0	0	90.18 ± 0.20
13	0	0	−1.73	93.41 ± 0.29
14	0	+1.73	0	89.29 ± 0.14
15	−1.73	0	0	70.23 ± 0.50
16	−1	+1	+1	67.17 ± 0.49
17	0	0	0	89.51 ± 0.58
18	0	−1.73	0	68.89 ± 0.41
19	+1	−1	+1	93.41 ± 0.09
20	0	0	0	90.28 ± 0.25

*Values are represented as mean ± SD ($n = 3$)

Preparation of MPLC-loaded soft nanoparticles (MPLC SNPs)

The MPLC SNPs were prepared by the nanoprecipitation method reported previously [45]. Briefly, MGN (10 mg) or MPLC (equiv. to 10 mg of MGN) was accurately weighed and mixed with dichloromethane (10 mL) using a magnetic stirrer until a clear solution was obtained. It was then introduced dropwise (0.2 mL/min) into a magnetically stirred distilled water (40 mL). The dispersed

Table 1 Coded levels and real values for each independent variable studied

Variables	Levels				
	−1.73	−1	0	+1	+1.73
Independent	Real values				
MGN:Phospholipon® 90H ratio (X_1, w:w)	1: 0.51	1:1.02	1:1.76	1:2.50	1:3.00
Reaction temperature (X_2, ^{0}C)	40.14	44.2	50.15	56.1	60.15
Reaction time (X_3, h)	1.01	1.42	2.01	2.6	3.00
Dependent					
Extent of complexation or yield (Y, % w/w)					

phase was then gradually evaporated while stirring, resulting in the formation of MGN SNPs or MPLC SNPs suspension with light green opalescence. The resultant suspension was then freeze-dried using a lyophilizer (Model: MSW-137, Macro Scientific Works Pvt. Ltd., New Delhi, India) under the conditions of controlled condenser temperature of − 80 °C and vacuum of 10 Pa. Finally, the lyophilized MPLC SNPs were stored in amber-colored (light-protected) glass vials, flushed with N_2, and kept at 4 °C until further use. The MGN SNPs (free of MPLC) were also prepared using the same procedure, stored, and evaluated.

Estimation of encapsulation efficiency and drug loading

A method previously described by Sahni et al. [53] and Alam et al. [54] was used for the estimation of drug loading and encapsulation efficiency of MGN within MPLC SNPs formulations, before and after lyophilization. Briefly, the prepared MPLC SNP suspension was transferred into a clean Eppendorf® Safe-Lock microcentrifuge tube (1.5 mL) and ultracentrifuged at 15,000 rpm at 4 °C for 40 min. The supernatant was collected, diluted suitably, and analyzed for the absorbance of the final solution at (λ_{max}, ~259 nm) using a UV-visible spectrophotometer. The encapsulation efficiency and drug loading were calculated using the equations described below:

$$Encapsulation\ efficiency\ (\%) = \frac{Total\ amount\ of\ MGN - Free\ MGN}{Total\ amount\ of\ MGN} \times 100 \quad (3)$$

$$Drug\ loading\ (\%) = \frac{Total\ amount\ of\ MGN - Free\ MGN}{Weight\ of\ nanoparticles} \times 100 \quad (4)$$

Physicochemical characterization of MPLC and MPLC SNPs

Scanning electron microscopy (SEM)

The comparative surface morphology of pure MGN, MPLC, and MPLC SNPs formulations was studied using a scanning electron microscope (Model: Supra®55, Carl Zeiss NTS Ltd., Germany). Briefly, the sample for SEM (scanning electron microscopy) analysis was prepared by weighing an individual sample (~ 50 mg) and spread uniformly over the double-sided carbon tape attached to the sample holder. Loaded samples were sputter-coated using a thin layer of gold (~ 400^0) and then examined under the microscope at an accelerating voltage of 10 kV. The captured images at different magnifications were read by the attached software (Smart®SEM V05.06).

Particle size and zeta potential

The particle size and size distribution of MGN in MPLC and MPLC SNPs were analyzed using Photon Cross-Correlation Spectroscopy (PCCS) equipped with dynamic light scattering (DLC) technique reported earlier by us [55]. Briefly, MPLC or MPLC SNPs (~ 5 mg) were accurately weighed and dispersed in deionized water (10 mL). The aqueous dispersion was then placed in the sample chamber of particle size analyzer (Model: NANOPHOX Sympatec, GmbH, Clausthal-Zellerfeld, Germany). The particle size analysis (range: 1 nm to 10 μm) was carried out by adjusting the sample vial position for optimizing the count rate as determined by the software. The resultant aqueous dispersion of MPLC or MPLC SNPs was used similarly for measuring the zeta potential using a Nano Particle Analyzer (Model: NanoPlusTM-2, Particulate system, Norcross, GA, USA) loaded with dynamic light scattering (DLS) setup. A complete analysis was carried out at RT with a sensitivity range of – 200 to + 200 mV.

Thermal analysis

The thermal behavior of the formulation components such as pure MGN, Phospholipon® 90H, the physical mixture (PM) of MGN and Phospholipon® 90H, and MPLC was comparatively analyzed by differential scanning calorimeter (DSC) and thermogravimetric analysis (TGA) (Model: DSC-1821e, Mettler-Toledo AG, Analytical, Schwerzenbach, Switzerland) as per the protocol reported by us earlier [56]. Briefly, the DSC was calibrated using high-purity standard indium (In) concerning heat flow and heat capacity. The sample analyzing area was continuously purged with dried N_2 at a flow rate of 50 mL/min. The samples (2.0 ± 0.2 mg each) were accurately weighed and subjected to heating in the range of 40 to 400 °C at a rate of 10 °C/min. The generated data were analyzed and interpreted by the instrument software (Universal Analysis 2000, V4.5A, Build 4.5.0.5).

Fourier-transform infrared spectroscopy (FT-IR)

Pure MGN, Phospholipon® 90H, PM of MGN and Phospholipon® 90H, and MPLC were analyzed by the FT-IR spectrophotometer (Model: FTIR-8300, Shimadzu, Kyoto, Japan) according to the previously reported protocols [57]. Briefly, a homogenous mixture of previously air-dried samples (~ 2 mg) with FT-IR grade potassium bromide (KBr,~ 200 mg) in an agate mortar and pestle was prepared, followed by compression into a thin transparent disc using Mini Hand Press Machine (Model: MHP-1, P/N-200-66,747-91,

Shimadzu, Kyoto, Japan) at a pressure of 10 ton/Nm^2. The prepared sample discs were scanned at a wavenumber range of 4000 to 400 cm^{-1}. The scanning resolution was fixed at 4 cm^{-1}. After scanning, the obtained individual sample spectra were interpreted using the peaks assigned by the FT-IR software (IR solution, version 1.10).

Powder X-ray diffraction (PXRD)

The comparative crystalline nature of the four samples pure MGN, Phospholipon® 90H, PM, and the MPLC was analyzed using a powder X-ray diffractometer (Model: D8 ADVANCE, Bruker AXS, Inc., Madison, WI, USA). The PXRD spectra of the samples were recorded on a 2θ scale according to a previously reported procedure [30].

Proton nuclear magnetic resonance spectroscopy (1H-NMR)

The ^{1}H-NMR spectra of formulation components, i.e., pure MGN, Phospholipon® 90H, and optimized MPLC formulations, were analyzed to study their carbon-hydrogen framework using a 400-MHz FT-NMR spectrophotometer (Model: Bruker Advance II, Bruker, Rheinstetten, Germany). The analysis was carried out at room temperature.

Solubility studies

The solubility of pure MGN, MGN SNPs, PM of MGN, and Phospholipon® 90H, MPLC, and MPLC SNPs was determined using a method previously described by Singh et al. [50]. Briefly, the samples were added in an excess amount to a sealed glass vial containing either purified water (5 mL) or 1-octanol (5 mL) which was further agitated using a shaker (Model: RSB-12, Remi House, Mumbai, India) for 24 h. The resulting dispersion was then centrifuged at 1500 rpm for 25 min. The supernatant was filtered using a 0.45-μ membrane filter to get a clear solution. The aliquot was suitably diluted using purified water or methanol and the absorbance of the solution was recorded to quantitate MGN (λ_{max}~259 nm) on a UV-visible spectrophotometer. The solubility analysis was conducted at RT.

Functional characterization of MPLC and MPLC SNPs

In vitro dissolution studies

The comparative in vitro dissolution profile of MGN suspension, MGN SNPs, MPLC, or MPLC SNPs was analyzed using a previously reported method [58]. Briefly, the dialysis membrane (LA395, dialysis membrane-110, HiMedia Laboratories, Mumbai, India) with an average diameter of ~ 21.55 mm, average flat width ~ 32.34 mm, and capacity ~ 3.63 mL was used for the dissolution study. The molecular size cutoff was 12,000–14,000 Da. The membrane was washed and rinsed according to the manufacturer's guidelines. Furthermore, the dialysis bags were prepared and the formulation samples such as MGN suspension (containing ~ 2 mg of MGN), MGN SNPs (~ 2 mg of MGN), MPLC (~ 2 mg of MGN), or MPLC SNPs (~ 2 mg of MGN) were placed into the dialysis bags and tied up with the thread. The bags were then suspended vertically into a beaker filled with dissolution medium, i.e., phosphate-buffered saline (PBS, 200 mL, pH 7.4) with Tween® 20 (1%, *v*/v). The contents of the beaker were continuously stirred (50 rpm, 37.0 ± 2.0 °C, 12 h) using a magnetic stirrer. Samples (5 mL) were withdrawn at regular intervals while maintaining the sink conditions. The samples were suitably diluted and the absorbance recorded ($_{max}$ ~ 259 nm) using UV-visible spectrophotometer. The cumulative amount of MGN released from the respective formulations was determined from the measured absorbance.

Ex vivo permeability studies

The comparative permeation efficiency of MGN from MGN SNPs and MPLC SNPs across a biological membrane was evaluated using an *everted rat intestine*, as described previously [55, 56, 59]. The study was performed using the intestine isolated carefully from albino rats of either sex with (150–200 g). On the day of the experiment, the overnight fasted animals were euthanized using a cervical dislocation method. The abdomen was incised carefully and the ileocecal part of the intestine was removed. The jejunal section of the intestine around ~ 7-cm long was carefully separated without any damage. The tissue was continuously washed with the freshly prepared Krebs solution. The intestine was then everted using a well-established, glass-rod procedure, described previously by Hamilton and Butt [60]. The everted intestine was kept in the freshly prepared Krebs solution until the permeation experiment.

The tissue was carefully mounted between the two tapered ends of the apparatus. Subsequently, the apparatus was filled with the freshly prepared Krebs solution and inserted carefully in a vertical position in a 250-mL beaker. The beaker was filled with the sample solution, MGN SNPs (100 μg/mL), or MPLC SNPs formulations (100 μg/mL) prepared in the Krebs solution. The whole assembly was placed on a magnetic stirrer and the contents of the beaker are stirred continuously at 25 rpm (37 ± 0.5 °C) for a period of 12 h. The Krebs solution in the apparatus as well as in the beaker was under constant aeration. At pre-determined intervals, samples were withdrawn and diluted appropriately, and the absorbance at (λ_{max} ~ 259 nm) is recorded using a UV-visible spectrophotometer. The apparent permeability was calculated by Eq. 5:

$$\text{Apparent permeability} = [V/(A \times T)] \times c_1/c_0 \quad (5)$$

where V represents the volume of serosal content (mL); A, the surface area of the intestinal sac (cm^2); T, time of incubation (sec); c_0, the initial concentration of on the mucosal side; and c_1, the concentration on the serosal side after time T.

In vivo antioxidant studies

The antioxidant potential of MGN SNPs and MPLC SNPs was evaluated in albino rats (male or female) using the CCl_4-induced oxidative stress model reported previously [58, 61].

Animals

Male and female albino rats (Wistar strain, bred in-house) weighing 150–200 g were used. The animals were kept under controlled conditions of temperature (25 ± 5 °C) and relative humidity (50 ± 5 %RH) with a 12-h light/dark cycle. They were nourished with pellet chaw (Brooke Bond, Lipton, India) and water ad libitum. The Institutional Animal Ethical Committee (IAEC) of Smt. Kishoritai Bhoyar College of Pharmacy, New Kamptee, Nagpur, sanctioned and approved the experimental protocols (*SKBCOP/IAEC/2017–2018, dated August 13, 2018*) for the current study. The studies were carried out according to the ethical guidelines available by the Committee for Purpose of Control and Supervision of Experiments on Animals (CPCSEA).

Dosing

The animals were divided randomly into four groups of six animals each. Group I animals received only Tween® 20 (1% *v*/v, p.o.) for 7 days and served as blank negative control. Group II animals also received Tween® 20 (1% v/v, p.o.) for 7 days. On the seventh day, group II animals received a single dose of a mixture of CCl_4 and olive oil (1:1, 5 mL/kg, i.p.) and served as a positive control. Group III animals received pure MGN SNP suspension at a dose of ~ 60 mg/kg of MGN, p.o., in distilled water with Tween® 20 (1%, v/v, p.o.) for 7 days. Group IV received MPLC SNPs at a dose of ~ 60 mg/kg of MGN, p.o., in distilled water with Tween® 20 (1%, v/v) for 7 days. After administration of the respective formulations to the animals, on the seventh day, the same groups also received a single dose of a mixture of CCl_4 and olive oil (1:1, 5 mL/kg, i.p.).

On the eighth day, the animals with CCl_4 intoxication were anesthetized using light ether anesthesia. The blood samples were collected from the retro-orbital plexus into tubes containing heparin and then centrifuged using a microcentrifuge (Model: RM-12C, Angle Rotor Head, Remi House, Goregaon (E), Mumbai, India) to obtain clear plasma samples. These were then used for the estimation of liver marker enzyme (liver function tests). Afterward, all the animals were euthanized by cervical decapitation and their livers were removed immediately and washed in ice-cold saline solution. The isolated livers were homogenized in 0.1 M PBS (pH 7.4) and then centrifuged to get a clear supernatant, which was further used for the estimation of antioxidant marker enzymes.

Liver marker enzyme estimation (liver function test)

The liver function marker enzymes such as serum glutamic oxaloacetic transaminase (SGOT), serum glutamic pyruvic transaminase (SGPT), alkaline phosphate (ALP), and total bilirubin were measured quantitatively to compare the influence of pure MGN SNPs and MPLC SNPs on liver function of the rats. The SGOT and SGPT in rat plasma were evaluated by the previously outlined method [62]. Briefly, SGOT substrate (0.5 mL) [α-L-alanine (200 mM) and SGPT substrate (0.5 mL) [L-aspartate (200 mM) with 2 mM α-ketoglutarate] were added in a clean test tube and incubated for 5 min at 37 °C. After incubation, the investigational rat plasma samples (100 μL) were added into the respective test tubes and the final volume was adjusted to 1 mL using phosphate buffer (pH 7.4, 0.1 M). The prepared mixture was then incubated further for 60 min (SGOT) or 30 min (SGPT) followed by the addition of 2,4-dinitrophenyl hydrazine as an indicator and incubated again for an additional 30 min. Following this, the freshly prepared sodium hydroxide solution (5 mL, 0.4 N) was added and the absorbance is measured at 505 nm.

The Grifols-Lucas method previously reported by Kind and King [63] was used to determine the ALP levels in the rat plasma. Briefly, the reaction mixture was prepared by the addition of phenyl phosphate buffer (1 mL, 0.5 N) to bicarbonate buffer (1 mL, pH 10) and then incubated at 37 °C for 3 min. To this solution, a rat plasma sample (100 μL) was added and incubated further for 30 min. Subsequently, the freshly prepared sodium hydroxide (0.8 mL, 0.5 N), $NaHCO_3$ (1.2 mL, 0.5 N), and amino-antipyrine (1 mL, 0.6%) solutions were introduced in the above reaction mixture and mixed well. The absorbance of the final solution was recorded at 520 nm.

Total bilirubin was determined from rat plasma using a previously reported method [64]. Briefly, in a test tube containing rat plasma (250 μL), the sulfanilic acid solution (5 mL, 4 mmol/L) and $NaNO_2$ (0.1 mL, 144 mmol/L) were added and the contents incubated at 37 °C for 10 min. After incubation, the absorbance was recorded at 670 nm.

In vivo antioxidant marker enzyme estimation

The antioxidant status of pure MGN SNPs and MPLC SNPs was assessed by measuring its influence on in vivo antioxidant

marker enzymes, viz., glutathione peroxidase (GSH), superoxide dismutase (SOD), catalase (CAT), and lipid peroxidase (LPO) present in the prepared rat liver homogenate. The antioxidant marker GSH was quantitatively determined using a well-known method [65]. Briefly, the reaction mixture was prepared by the addition of liver homogenate supernatant (200 μL), distilled water (1.8 mL), and precipitating mixture (0.3 mL) to a clean test tube, mixed well and centrifuged by using a microcentrifuge at 5000 rpm for 5 min to get clear supernatant, 1 mL of which was mixed with phosphate buffer (1. 5 mL, 0.1 M) and 5,5′-dithiobis-(2-nitrobenzoic acid) (DTNB, Ellman's reagent, 0.5 mL). The resulting solution was analyzed for absorbance at 412 nm. The obtained value was expressed as μg/mg of protein.

In the rat liver homogenate, the SOD level was estimated as described previously [66]. Briefly, in a test tube containing liver supernatant (20 μL), Tris-HCl buffer (2 mL, 75 mM, pH 8.2) and freshly prepared pyrogallol solution (0.5 mL, 30 mM) were mixed. The resultant solution was recorded for an increase in absorbance for 3 min. at an interval of 30 s. at 420 nm. The rate of auto-oxidation of the pyrogallol solution with 50% inhibition by SOD was considered as one unit enzyme activity. The value was expressed as units/mg of protein.

A method earlier described by Stocks and Dormandy [67] was employed for the estimation of LPO in the prepared liver homogenate. Briefly, to rat liver supernatant (500 μL), the freshly prepared sodium lauryl sulfate (0.2 mL, 0.8% *w/v*), trichloroacetic acid (1 mL, 20% w/v), and thiobarbituric acid (1.5 mL, 0.85 w/v) were added, mixed, and then heated at 100 °C for a period of 1 h. The solution was cooled to RT and diluted with distilled water (1 mL). The mixture was centrifuged to separate the organic layer from the aqueous one. The organic layer was carefully collected in a cuvette and its absorbance is measured at 532 nm. The molar extinction coefficient of malondialdehyde (MDA) (1.56×10^5 M^{-1} cm^{-1}) was used for the calculation of lipid peroxidation. The LPO enzyme activity was expressed as MDA (nM/g) in hemoglobin.

Similarly, the CAT enzyme level in the liver supernatant was determined using the method described by Beers and Sizer [68]. Briefly, the prepared liver supernatant (100 μL) was mixed with phosphate buffer (1.9 mL, 50 mM, pH 7.4) and the freshly prepared H_2O_2 solution (1 mL, 30 mM). This mixture was then analyzed at 240 nm. The enzyme activity was correlated with the extent of H_2O_2 decomposition.

Histopathological studies

At the end of dosing of formulations and CCl_4 intoxication, all the animals were euthanized by cervical decapitation method. Subsequently, their livers were removed immediately, washed in ice-cold saline, and preserved in a neutral buffered formalin (10% *v*/v) solution till further processing. The livers were sectioned and stained using a hematoxylin-eosin reagent. The stained sections were observed under an optical microscope (Model: DM2500, Leica Microsystems Inc., Buffalo Grove, IL). The observed and suitable images were captured using an attached digital camera at a magnification of × 400.

Oral bioavailability studies

Bioanalytical method development

Method development was started by preparing the stock solution of standard MGN. Briefly, an approximate amount of MGN (~ 10 mg) was dissolved in sufficient amount of methanol and the solution with a concentration of 1000 μg/mL is prepared. The prepared solution was stored at 4 °C until analysis. From this, different concentrations of solutions were prepared and spiked with blank plasma to get the final solution in the range of 0.05–10 μg/mL, respectively. These solutions were used for the preparation of quality control (QC) samples at a concentration of low (0.05 μg/mL), medium (0.5 μg/mL), and higher (10 μg/mL), respectively. In these solutions, the freshly prepared nitrophenol as internal standard (IN, 4 μg/mL) and a 3 mL of acetonitrile were added and mixed well. The developed reaction mixture solution was vortexed and then centrifuged at a condition of 800 × g for 10 min to get clear supernatant. The obtained supernatant was collected, evaporated, and reconstituted using 100-μL mobile phase. This solution was injected into HPLC (Thermo ScientificTM UltimateTM 3000, Thermo Scientific, San Jose, CA, USA), the peak areas of standard plasma spiked with various concentration of MGN are determined, and then the ratio of peak areas of IN and MGN against the concentration of MGN is plotted. Following this, the calibration curve was prepared and linearity was calculated.

A chromatographic method described earlier by Chen et al. [69] was also followed for the quantification of MGN in the collected plasma samples. Briefly, the MGN estimation in plasma was carried out using the same HPLC system as mentioned in the above method development section. This system is equipped with a photodiode array detector (Thermo Scientific, San Jose, CA, USA). The stationary phase consisted of the Hypersil GOLD™ C18 selectivity LC column (100 × 4.6 mm) with a particle size of 5 μm. Acetonitrile and acetic acid (3%) in MiliQ water were used as the mobile phase for gradient elution. During the entire analysis, the flow rate of the optimized mobile phase as well as the column temperature was maintained at 1.0 mL/min and 30 °C, respectively. The detection was performed at 259 nm. Nitrophenol was used as an IN due to its structural similarity to MGN. The optimized mobile phase was used for the effective resolution of MGN peaks in the HPLC chromatograms. The peaks were analyzed and interpreted using a software associated with the HPLC system.

Extraction of MGN from plasma and sample preparation

The extraction of MGN from rat plasma was carried out by the liquid-liquid extraction (LLE) method described previously [61]. The LLE exhibits high recovery and reproducibility from the biological matrix. Briefly, male and female albino rats were divided into two groups containing six animals each (overnight fasting with free access to water). Group I animals received pure MGN SNP suspension at a single dose of ~ 60 mg/kg of MGN, p.o., and group II received MPLC SNPs (~ 60 mg/kg, p.o. of MGN). Afterward, the animals were anesthetized at designated time intervals, and then blood samples were collected from their retro-orbital plexus. Collected blood samples were transferred into clean heparinized Eppendorf® Safe-Lock microcentrifuge tubes (1.5 mL). The tubes containing samples were centrifuged at 800 *g* for 10 min. to separate the plasma, which was stored at − 20 °C till further analysis.

The MGN from plasma samples was extracted by spiking plasma samples (500 μL) of respective formulations with 20 μL of IN and of acetonitrile (3 mL). The mixture was vortexed for 1 min and centrifuged at 800 *g* for 10 min. The supernatant was carefully collected and transferred to another clean tube. The solvent was allowed to evaporate in a vacuum desiccator and then the residue reconstituted (mobile phase, 100 μL). A 20-μL sample was injected for the quantitation of MGN.

Validation of the extraction and quantification method

The guidelines as suggested by the International Conference on Harmonization (ICH) were used for carrying out validation of the developed HPLC method. The validation parameters, i.e., intra-day accuracy and precision, were determined for prepared QC samples on the same day ($n = 6$), while, inter-day accuracy and precision were determined for the same QC samples on three following days. Moreover, the extraction recoveries of MGN from extracted tissue samples and standard solutions at the same concentration were tested and compared. The short-term (for 24 h) and long-term (for 14 days) stability studies were also performed on QC samples.

Study of pharmacokinetic parameters

The pharmacokinetic parameters such as C_{max} and T_{max} were determined from the plasma concentration time profile. Other parameters such as half-life ($t_{1/2}$), area under the plasma concentration time curve (AUC) from zero to time of final measured sample ($AUC_{0\text{-}t}$) and from zero to infinity ($AUC_{0\text{-}\infty}$), clearance (Cl/F), the volume of distribution, and relative bioavailability (F) were estimated using WinNonlin® statistical software (Version 4.1, Certara USA Inc., Princeton, NJ, USA).

Stability studies

According to the ICH guidelines, the long-term stability studies were carried out on lyophilized MPLC SNPs formulations. Briefly, the lyophilized formulation was sealed in clear glass vials and stored at RT (25 °C) and 4 °C, respectively, for the period of 6 months. At designated intervals (i.e., 0, 3, and 6 months), the samples were removed and analyzed for particle size, PDI, zeta potential, and entrapment efficiency of MPLC SNP formulations.

Statistical analysis of data

The results of solubility and in vitro dissolution and stability studies were reported as mean ± standard deviation (SD). Similarly, the results of liver function tests, the in vivo antioxidant activity, and pharmacokinetic studies were represented as mean ± standard error of the mean (SEM). One-way analysis of variance (ANOVA) followed by Dunnett's test was used for estimating the statistical differences between treatment groups. An obtained P value < 0.05 was considered to be statistically significant.

Results and discussion

Formulation of MPLC and MPLC SNPs

MGN is a well-known xanthonoid exhibiting fair solubility in most organic solvents and poor solubility in water [18, 21]. The present study aimed at improving the aqueous solubility of MGN by incorporating it in the form of MPLC. We and others have previously shown that the flavonoid-phospholipid complexes could be successfully prepared by using 1,4-dioxane [30], CH_2Cl_2 [19], and tetrahydrofuran (THF) [70] (solvent evaporation method). Based on these studies, we have also used these solvents for the preparation of phospholipid complex. However, while preparation, we found that both MGN and phospholipids exhibited poor solubility in the abovementioned solvents, which further results in precipitation of both the formulation components. To overcome these inherent solubility issues, we tested other organic solvents for the solubilization of MGN and phospholipids. Out of all the solvents tried, absolute ethanol showed better suitability. Given the semi-polar nature of this class III solvent with a low-toxicity profile, we chose to formulate MGN with phospholipids using ethanol as a solvent with the hope that it would result in the stable MPLC formulation.

On the other hand, MPLC SNPs were prepared using dichloromethane as a solvent by the nanoprecipitation technique in four steps: (i) formation of o/w dispersion (of organic phase in continuous aqueous phase); (ii) dramatic reduction in the interfacial tension between the two phases, leading to the

lowered droplet size of MPLC; (iii) formation of soft nanoparticles due to evaporation of the organic solvent; and (iv) precipitation of nanodroplets from the aqueous environment with the formation of self-assembled MPLC SNPs.

The rationale for selecting independent, dependent variables and their ranges

Based on the preliminary experiments, the independent, dependent variables and their ranges were selected and used in the formulation of MPLC. It was prepared using a solvent evaporation method, and based on this, three independent variables were selected, i.e., MGN/Phospholipon® 90H ratio, reaction temperature, and reaction time. The ratio acts as the basic composition of MPLC. Reaction temperature helps in the establishment of a complex between MGN and Phospholipon® 90H, while reaction time provides the maximum contact between MGN and Phospholipon® 90H, resulting in the formation of stable MPLC. The extent of complexation was selected as the dependent variable. After the selection of these variables, their experimental ranges were selected. According to Semalty et al., the drug/Phospholipon® 90H ratio (1:1), reaction temperature (40 °C), and reaction time (1 h) are the suitable range for the successful preparation of phospholipid complex [71]. So, we utilized the same range for the preparation, resulting in the formation of MPLC with limited solubility and a low extent of complexation. To improve these parameters, we increased the MGN/Phospholipon® 90H ratio from 1:1 to 1:2, the reaction temperature from 40 to 50 °C, and the reaction time from 1 to 2 h, respectively, which resulted in the formation of various MPLCs with significant enhancement in its solubility and extent of complexation. However, to explore further the range of independent variables at various levels, we selected CCD as one of the best optimization tools, because it provides the chance to explore the largest possible processing space at five levels, i.e., extremely lower level (− 1.73), low (− 1), middle (0), higher (+ 1), and extremely higher level (+ 1.73), respectively. The obtained experimental trials by using these levels showed a significant impact on the response variables. Hence, we have chosen three independent variables and studied their range at five levels using CCD.

CCD

Table 2 lists the results of the extent of complexation or yield (%, *w*/w) for the respective experimental trial formulations of MPLC obtained using a combination of studied independent variables. As seen from Table 2, the yield (%) was in the range of 59.2 to 97.71%, indicating the significant impact of independent variables of MGN/Phospholipon® 90H ratio (X_1), reaction temperature (X_2), and reaction time (X_3) on the response variable. At the end of the formulation trials, the following polynomial equation (Eq. 6) was obtained. It was further used for formulation optimization. Moreover, the generated positive and negative (+ or −) signs associated with the coefficient of magnitude were also used to study the influence of independent variables on the yield as well as for the optimization of the same variables:

$$Y = 90.13 + 7.13X_1 + 0.0680X_2 + 2.54X_3 - 5.28X_1^2 - 5.15X_2^2 - 0.668X_3^2 + 1.90X_1X_2 - 03975X_2X_3 - 0.0425X_1X_3 \quad (6)$$

The output of the CCD trials, i.e., fit summary, ANOVA data, polynomial equation, counter, and 3D response graphs, was critically analyzed wherein the quadratic model was found to be the best-fit model. It correlated well with the polynomial equation. The coefficients b_1, b_{11}, and b_{12} were statistically significant ($p < 0.05$). Other coefficients b_0, b_2, b_3, b_{13}, b_{22}, b_{23}, and b_{33} were statistically non-significant. The model *F-value* (3.21) indicates the suitability of the quadratic model for experimental trial formulations. Additionally, the adequate precision value was greater than > 4 (i.e., 8.133) and the correlation coefficient value (R^2) between adjusted and predicted appeared less than < 0.2, which suggests that the quadratic model is the best-fit model, and therefore, this model can be used to navigate the design space. The model summary statistics showed that the PRESS value for response yield was ~ 4087.42, which also indicates the suitability of quadratic model as the best-fit model. The developed positive sign (+) in the coefficient of the magnitude of X_1, X_2, and X_3 showed that as the concentration of X_1, X_2, and X_3 increases, the yield also increases simultaneously, indicating a direct correlation between the independent and dependent variables. The overall influence of independent variables (X_1, X_2, and X_3) on yield is shown as counter and 3D response plot Fig. 1a and b. As seen in this figure, at constant reaction time, the yield was found to increase, as the X_1 and X_2 increase to the middle level and then decreased. Moreover, at the fixed reaction temperature, the yield increased, increasing the X_1 and X_3 to the middle level and then decreased. Also, at fixed MGN/Phospholipon® 90H ratio, the yield also increased, as the X_2 and X_3 increase to the middle level and then decreased, respectively. Therefore, it can be concluded that the middle values of X_1, X_2, and X_3 may be found as an optimal value for achieving higher yield.

The optimization of the suitable experimental trial with higher yield was achieved by following numerical and graphical optimization techniques. In both techniques, the constraints were applied to independent and dependent variables to get the desired and optimized formulation. The constraints for independent variables

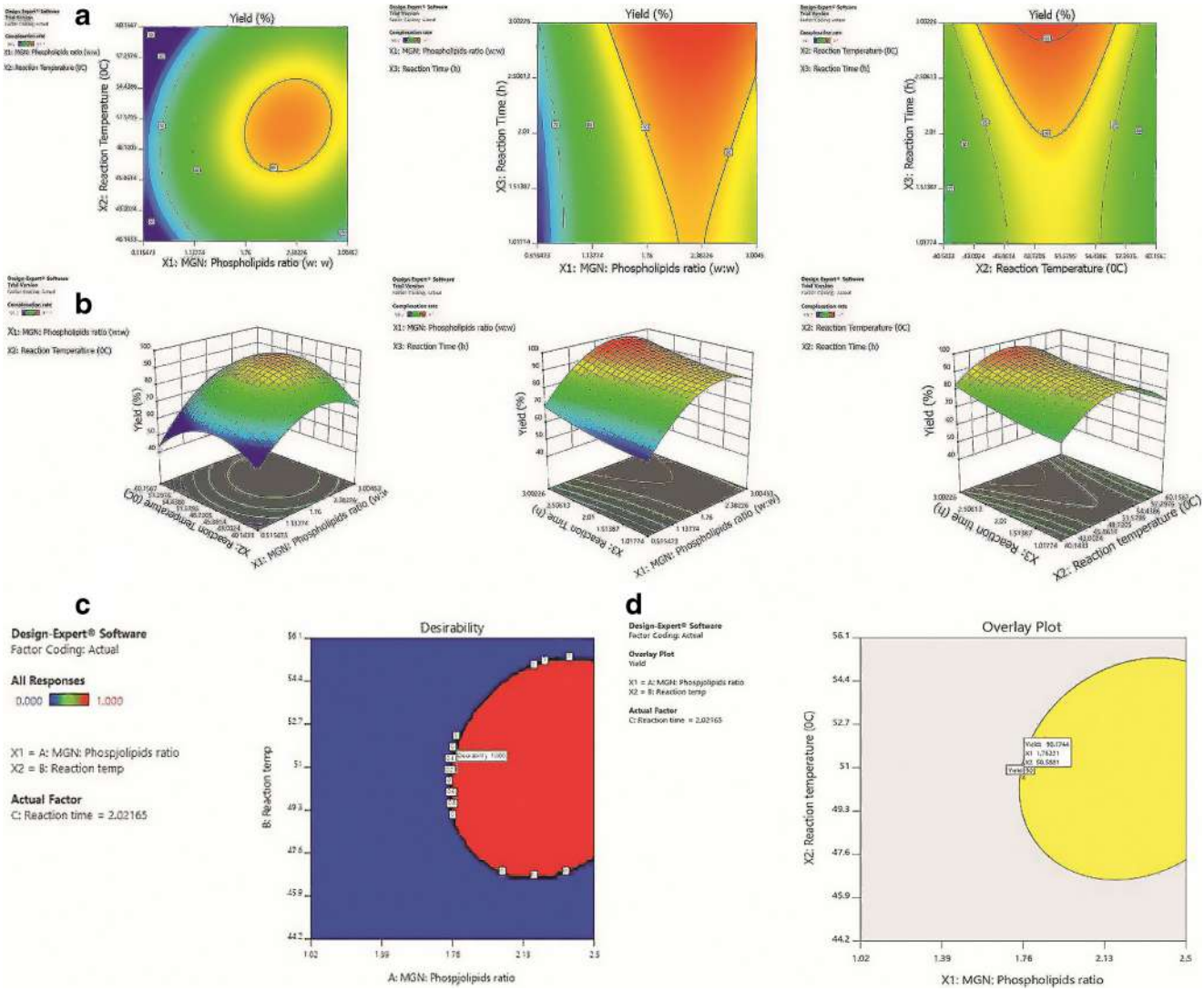

Fig. 1 **a** Contour plot, **b** 3D response surface plot, **c** desirability plots, and **d** design space of extent of complexation or yield (Y, %) as a function of MGN and Phospholipon® 90H ratio (X_1, w: w), reaction temperature (X_2, °C), and reaction time (X_3, h)

of X_1, X_2, and X_3 were in the range of 1:1.02 to 1:2.5 (w: w), 44.2–56.1 °C, and 1.42–2.6 h, whereas the constraints for yield were in the range of 90.0–96.10 (%, *w*/w), respectively. Following the analysis, the design provided one possible solution of the experimental trial, which showed recommended values of independent variables as well as desirability value close to 1. The results of this analysis are shown as desirability plot (Fig. 1c). In graphical optimization, the constraints used for yield were the same as that used in numerical optimization, and based on this, it showed the design space in the form of overlay plot (Fig. 1d). The suggested values of the design space were used for the preparation of optimized formulation. Overall, the combination of desirability and design space overlay plot provided the optimal values of ~1:1.76 (w:w), 50.55 (°C), and 2.02 (h) for the independent variables of MGN/Phospholipon® 90H ratio (X_1), reaction temperature (X_2), and reaction time (X_3), respectively.

Validation of model optimization

The validation of the CCD-generated model was carried out by preparing an additional trial formulation of MPLC using optimal values of X_1, X_2, and X_3. The actual yield of MPLC (~90.35%) was found in a close agreement with the predicted value (~90.14%). The experimental confirmation, in a way, validated the robustness of the design-generated quadratic model. The predicted error or bias (%) between these two yields was calculated using Eq. 7. It was found to be < 3% (0.21). Overall, the CCD helped in optimizing the MPLC formulation successfully:

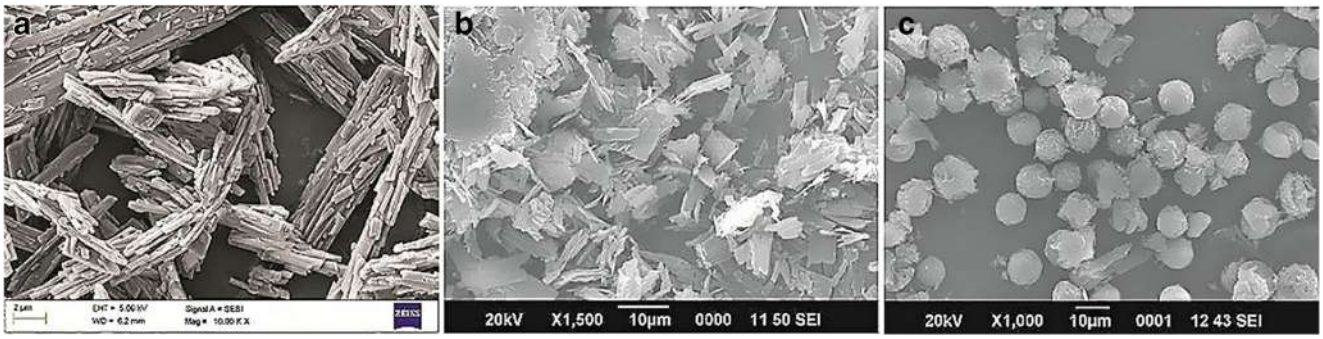

Fig. 2 SEM image of **a** pure MGN, **b** MPLC, and **c** MPLC SNPs formulations

$$Bias\ (\%) = \frac{predictedvalue - observedvalue}{predictedvalue} \times 100 \qquad (7)$$

Physicochemical characterization of MPLC and MPLC SNPs

SEM

The SEM analysis of pure MGN, MPLC, and lyophilized MPLC SNPs formulations is shown in Fig. 2a, b, and c, respectively. The particles of pure MGN (Fig. 2a) appeared as a blend of small and large needle-shaped particles with ill-defined edges. SEM image of optimized MPLC in (Fig. 2b) exhibited as large, fused, and irregularly shaped particles with heterogenous surface suggests the formation of a complex between pure MGN and Phospholipon® 90H. Compared with pure MGN and MPLC, the SEM morphology of lyophilized MPLC SNPs (Fig. 2c) appeared as spherical shaped particles with heterogenous surface, suggesting that the implementation of nanoprecipitation coupled with lyophilization technology could result in the formation of spherical particles.

Particle size and zeta potential

The physical stability of the sub-micron particles in a liquid medium is mostly dependent on two parameters—particle size distribution and zeta potential. Previously, Telange et al. prepared apigenin-phospholipid complex (APLC) and reported particle size and PDI value around ~ 107.08 ± 1.30 nm and 0.37 as narrow particle size distribution. The APLC enhanced aqueous solubility and bioavailability following oral administration [30]. The same author also developed umbelliferone-phospholipid complex (UPLC) and its particle size and PDI values were found to be higher around ~ 7134.79 ± 0.67 nm and 0.53. The UPLC with these parameters significantly enhanced the solubility, permeation, and anti-inflammatory potential of umbelliferone [48]. Figure 3a shows the particle size distribution of MPLC with mean particle size of 507.55 ± 0.40 nm and polydispersity index (PDI) of 0.43 ± 0.10, indicating relatively wide particle size distribution of MGN within MPLC However, upon comparison with APLC and UPLC, the particle size and PDI value of MPLC was found to be in between them, suggesting that MPLC particles are acceptable smaller particle size and thus found to be suitable for oral administration. Moreover, the particle size of pharmaceutical processed materials is found to be inversely proportional to their surface area/volume (SA/V) ratio, which means that the smaller the particle size, the higher is the SA/V. This concept is found to apply to MPLC, as the smaller particle size of MPLC shows a higher SA/V ratio, resulting in increased solubility and release rate of MGN from MPLC via diffusion and surface erosion [72]. It is well accepted that smaller particles (size < 500 nm) are usually taken up by endocytosis during their transit across the biological membranes. In contrast, larger particles < 5 mm are easily absorbed by the lymphatic system [73, 74].

Zeta potential (ζ) is yet another significant measure specifically used for the determination of surface charges (+ or −). This has a direct impact on the physical stability of the multiparticulate systems. Earlier reports have suggested that zeta potential of values greater than ± 10 mV is indicative of considerable physical stability of the multiparticulate systems [75, 76]. The measured zeta potential of the optimized MPLC formulations is shown in (Fig. 3b). The observed value of zeta potential of MPLC formulations was found to be − 12.53 ± 0.17 mV, which is higher than − 10 mV, indicating a physical stability of MPLC formulations The obtained zeta potential value of MPLC could potentially be attributed to the small portion of phospholipids involved in the complexation process with the generation of negative charges in an aqueous environment with near-neutral pH value This mechanism could provide sufficient negative charges on the surface of MPLC, making it considerably stable in the aqueous state. Moreover, the phospholipid composition and its type may also influence the zeta potential values significantly [30]. Therefore, the results demonstrated that the MPLC formulation of better physical stability was obtained.

Similarly, the measured particle size distribution and zeta potential of MPLC SNPs are shown in Fig. 3c and d, respectively. Lyophilization of the MPLC SNPs was carried out using

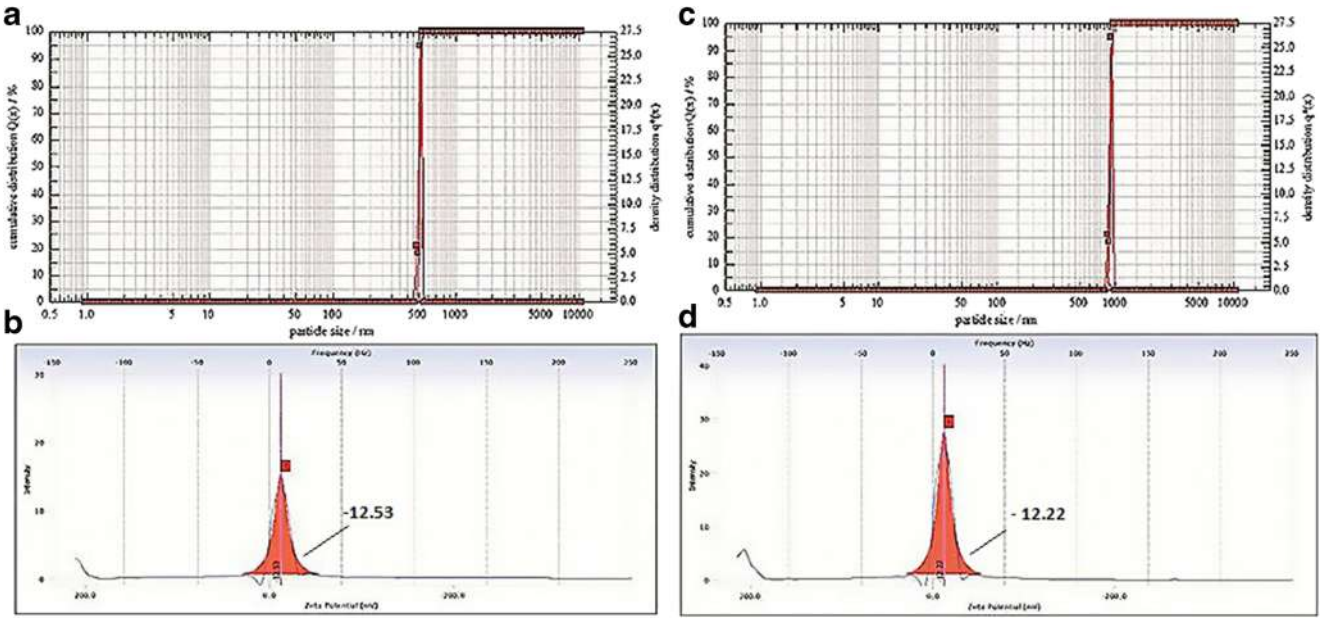

Fig. 3 **a** Particle size distribution, **b** zeta potential of the optimized MPLC formulation before lyophilization, **c** particle size distribution, and **d** zeta potential of MPLC SNPs after lyophilization

sucrose (2% *w*/w) as cryoprotectant. The formulation exhibited higher average particle size and PDI value of 906.69 ± 0.20 nm and 0.50 ± 0.19, respectively (Fig. 3c). The zeta potential of the lyophilized formulation was comparable to the one before lyophilization, i.e., − 12.22 ± 0.33 mV (Fig. 3d), indicating that the lyophilization technique preserved the physical, chemical, and, most likely, biological stability of the formulation. This is going to be beneficial by preventing the leakage of MGN from MPLC-loaded SNPs under realistic conditions of use in vivo. The results were found to be consistent with an earlier report [45]. Overall, the comparative results of particle size, PDI, and zeta potential values before and after lyophilization are shown in Table 3.

In this study, the MPLC SNPs were prepared using the nanoprecipitation method followed by lyophilization. Lyophilization is the most widely used method which converts solution or suspension into a lyophilized solid form with improved stability and particle size of nanoparticles. However, the freezing, primary drying, and secondary drying steps of the lyophilization process may create stressful conditions (i.e., formation of ice crystal and particle aggregation via crystallization) that can result in destabilization of nanoparticles. To reduce this mechanical stress as well as increase the stability of nanoparticles, the optimization of the lyophilization process is needed and it is done by introducing the cryoprotectant, which can act as protective agents and prevents the aggregation and/or fusion of nanoparticles during lyophilization and enhances its stability. The same optimization was also carried out for MPLC SNPs using various cryoprotectants at different concentrations. According to earlier reported studies, the total seven cryoprotectants, i.e., glucose, fructose (as monosaccharides), trehalose, maltose, and sucrose (as disaccharides), PVA, and PVP (as a polymer) were studied at four concentrations of 0.5, 1, 2 and 5% (*w*/w), respectively, and investigate their effect on particle size and PDI of MPLC SNPs [77]. In the following analysis, the PVP and PVA at all concentration range significantly increased the particle size and PDI value of MPLC SNPs around ~ 941.10 and ~ 0.74 nm, respectively. It may be attributed to the complete absence of a thick layer of this polymer at these concentrations on the surface of nanoparticles, which causes the fusion of particles and increases the particle size and PDI values of MPLC SNPs [77]. After lyophilization, all monosaccharides at lower concentration (0.5 and 1%) maintain the same particle size and PDI value as that of polymer, while at higher concentration (2 and 5%), it marginally reduces the particle size

Table 3 Encapsulation efficiency, drug loading, particle size, PDI, and zeta potential values of MPLC SNPs formulations before and after lyophilization

MPLC SNPs formulations	Encapsulation efficiency (%)*	Drug loading (%)*	Particle size (nm)	PDI	Zeta potential (mV)
Before lyophilization	82.23 ± 0.37	17.48 ± 0.19	507.55 ± 0.40	0.43 ± 0.10	− 12.53 ± 0.17
After lyophilization	81.63 ± 0.41	16.91 ± 0.30	906.69 ± 0.20	0.50 ± 0.19	− 12.22 ± 0.33

*Data are represented as mean ± SD ($n = 3$)

around ~ 936.39 and ~ 0.68 nm, respectively, compared with polymer, suggesting that the crystallization of these excipients during lyophilization may lose its ability and/or form weak interaction with nanoparticles which results in lowering of particle aggregation to some extent and reduces the particle size and PDI value of MPLC SNPs [77]. Compared with polymer and monosaccharides, the trehalose and maltose at lower concentration (0.5 and 1%) displayed nearly about the same value as that of values shown by monosaccharides at lower concentration, i.e., ~ 939.06 and 0.70 nm, respectively, whereas, at higher concentration (2 and 5%), it marginally reduces the particle size and PDI value of MPLC SNPs around ~ 931.50 and ~ 0.62 nm, respectively, suggesting the solidification of these materials while lyophilization increases the interaction with nanoparticles and, thus, reduces the particle size and PDI value of MPLC SNPs [78, 79]. Among all disaccharides, the sucrose displayed best and more significant results. At lower concentrations, sucrose showed the same results as that of a lower concentration of disaccharides. At 5% concentration, sucrose marginally reduces the particle size and PDI value around ~ 923.42 and ~ 0.56 nm, respectively. However, sucrose at 2% concentration, after lyophilization, more appreciably reduces the particle size and PDI value of MPLC SNPs around ~ 906.69 and ~ 0.50, respectively, with the appearance of spherical shaped particles as shown in SEM studies. This significant result was likely due to the lyophilized amorphous nature of sucrose, which can form strong H-bonding interactions with developed nanoparticles, preserves it in pseudo-hydrated form, and improves stability of nanoparticles [80]. Moreover, the low hygroscopic nature of sucrose attracts the water molecules from the surrounding environment which form hydrogen bonding with nanoparticles, resulting in the reduction of the particle size and preserving the stability of nanoparticles [81]. Additionally, the phase transformation behavior of sucrose at higher temperatures could provide a favorable environment to lyophilization, forming a stable lyophilized amorphous cake, which shows high redispersibility, lower residual moisture content, and long-term stabilization on storage [82, 83]. Based on these results, the sucrose at 2% (*w*/w) was chosen as optimum cryoprotectant improving the stability, particle size, and PDI value of MPLC SNPs.

Encapsulation efficiency and drug loading

Encapsulation efficiency and drug loading analysis for the MPLC SNPs formulations before and after the lyophilization are presented in Table 3 with the respective values before lyophilization as 82.23 ± 0.37 and 17.48 ± 0.19%. However, after lyophilization, the MPLC SNPs exhibited no significant change in encapsulation efficiency (81.63 ± 0.41%) and drug loading (16.91 ± 0.30%). The results indicate that the adopted combined formulation strategy had no remarkable influence on the quite important encapsulation efficiency and drug content. This is very crucial since the potentially sustained drug release performance was without any sign of drug leakage.

Thermal analysis

Thermograms of pure MGN, Phospholipon® 90H, PM of pure MGN and Phospholipon 90H®, and the MPLC are depicted in Fig. 4a, b, c, and d, respectively. As seen from (Fig. 4a), pure MGN exhibited a sharp, high-intensity melting peak at 267.38 °C. Such sharp peaks are indicative of high purity and the crystalline nature of the substances. The peak was similar to the one reported previously [61]. Phospholipon® 90H showed multiple (#5) endothermic peaks (Fig. 4b). Out of the five peaks, the initial three low-intensity, broad, and diffused peaks (84.90, 107.99, and 179.91 °C) indicated the melting of the polar region of the phospholipids. The latter two peaks appeared at 209.66 and 334.43 °C, possibly due to thermal scrambling in the hydrophobic tails of the phospholipids leading to the transformation of the gel-like structure to a crystalline state. These observations were in agreement with the earlier reports [28, 47]. The PM thermograms showed four endothermic peaks at 86.67, 110.65, 179.91, and 265.42 °C (Fig. 4c). The first three peaks were contributed by Phospholipon 90H®, whereas the fourth peak was contributed by pure MGN, demonstrating the additive nature of pure MGN and Phospholipon 90H®. These peaks resulted from the melting of the PM at higher temperatures with the partial formation of the complex, which exhibited lower melting temperature compared with the original formulation. Moreover, the peak intensity of pure MGN in PM thermograms was lower compared with the corresponding peak in pure MGN. However, on close observation, it appeared that, like other small intensity peaks of Phospholipon® 90H, the low-intensity peak of MGN is also detected and this could be due to the remnant MGN while the major amount interacted with Phospholipon® 90H [84]. The thermogram of MPLC (Fig. 4d) displayed a new low-intensity endothermic peak at 82.11 °C, which was completely different from the original peaks observed for pure MGN and Phospholipon® 90H. Moreover, the sharp melting peak of MGN disappeared completely, indicating the amorphization of pure MGN [30, 72]. A completely different DSC melting behavior indicated the occurrence of weak intermolecular interactions such as H-bonding, van der Waals forces, or ion-dipole forces between pure MGN and Phospholipon 90H®. Thus, it is suggested that the formulation process completely dispersed MGN within the phospholipid matrix, leading to the formation of amorphous and stable MPLC [85, 86]. Moreover, the pure MGN and MPLC both exhibited enthalpy of fusion (ΔH) of 29.27 and 152.8 J/g, respectively. This observed difference in enthalpy of fusion for MGN and MPLC further confirmed the formation of the complex.

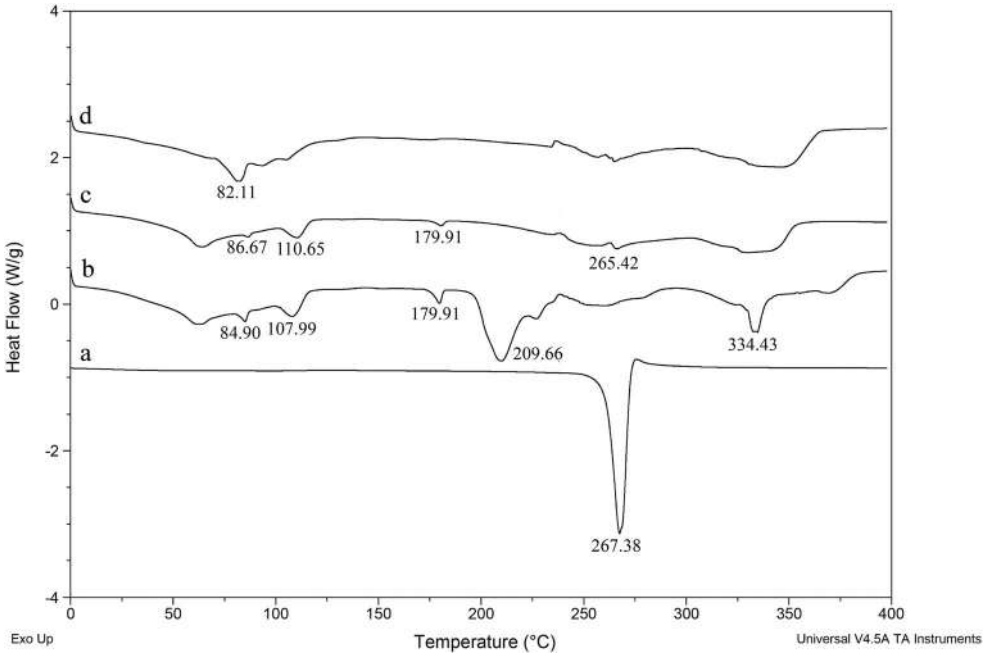

Fig. 4 DSC thermograms of **a** pure MGN, **b** Phospholipon® 90H, **c** the physical mixture (1:1.76) of pure MGN and Phospholipon® 90H, and **d** MPLC formulations

In addition to DSC, the thermogravimetric analysis (TGA) is yet another valuable technique also employed for the investigation of the thermal performance of the formulation. The TGA curves of pure MGN, Phospholipon® 90H, PM, and the MPLC are shown in Fig. 5a, b, c, and d, respectively. Pure MGN (Fig. 5a) exhibited a pointed decrease in weight loss (~ 10%) in the temperature range 250–275 °C, corresponding to the melting (endothermic peak) of pure MGN. Beyond 275 °C, a continued weight loss was observed, indicating the thermal degradation of MGN. The TGA curves of Phospholipon® 90H (Fig. 5b) displayed a sharp loss in weight (~ 90%) around 225 °C. Beyond this point, the curve showed consistent lowering. This could be attributed to the physicochemical transformation of the phospholipids from the gel-like structure to the crystalline state. Figure 5c showed the TGA curve of the PM. It displayed a weight loss (~ 105%) between the ranges of 225 and 350 °C. Beyond 350 °C, PM showed rapid weight loss. In contrast to this, MPLC (Fig. 5d) exhibited a weight loss (~ 125%) between the same ranges as mentioned for PM; however, on close observations; it was found that the MPLC beyond 350 °C exhibits slow rate of weight loss compared with rapid weight loss of PM, which

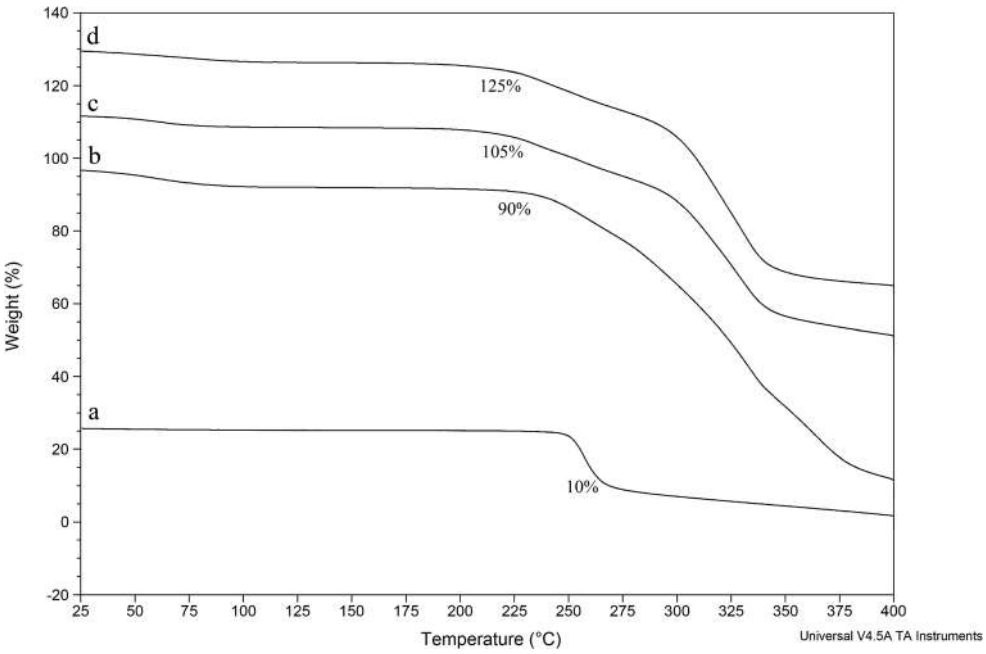

Fig. 5 TGA curves of **a** pure MGN, **b** Phospholipon® 90H, **c** the physical mixture (1:1.76) of pure MGN and Phospholipon® 90H, and **d** MPLC formulations

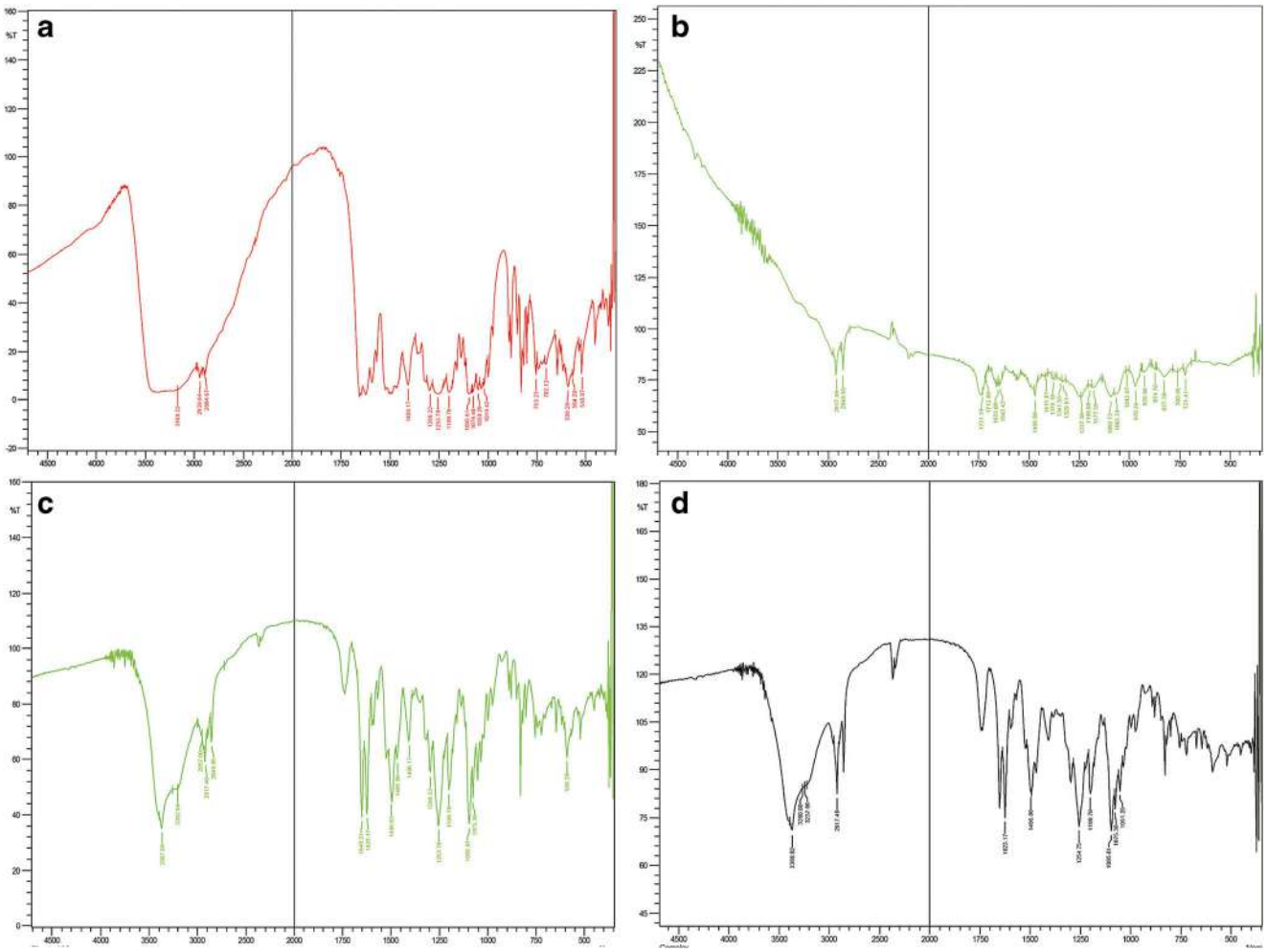

Fig. 6 FT-IR spectra of **a** pure MGN, **b** Phospholipon® 90H, **c** the physical mixture (1:1.76) of pure MGN and Phospholipon® 90H, and **d** MPLC formulations

indicates an improved thermal stability of MGN due to the formation of MPLC complex [87]. This result suggested that the molecular interaction of MGN with the polar head of Phospholipon® 90H via polar and hydrogen bonding interactions could increase their affinity toward each other and increase the stability of MPLC.

FT-IR

Figure 6 (a, b, c, and d) depicts the FT-IR spectra for pure MGN, Phospholipon® 90H, PM, and MPLC formulation, respectively. As seen in (Fig. 6a), pure MGN displayed distinctive absorption signals at 3367.86 and 3168.22 cm^{-1}corresponding to the O-H stretching, 2939.64 cm^{-1} for aliphatic C-H stretching, 1648.66 and 1622.56 cm^{-1} for C=O stretching, 1253.78 and 1095.61 cm^{-1} for aryl ether C-O-C stretching, 1406.17 cm^{-1} for C=C stretching, and 702.12 and 589.28 cm^{-1} for aromatic bending vibrations. These signals were consistent with the earlier published reports [61]. The FT-IR spectrum of Phospholipon® 90H (Fig. 6b) marked the presence of multiple characteristic absorption signals, which appeared at 2917.46 and 2849.95 cm^{-1} (C-H stretching of long fatty acid chain) and 1731.19 cm^{-1} for C=O stretching vibration of fatty acid ester. Besides these, some additional signals were also observed at 1237.39 and 1092.72 cm^{-1} (for P=O and P-O-C stretching) and 970.24 cm^{-1} for [$-N^{+}(CH_3)_3$]. These FT-IR peaks were in agreement with the previous reports for Phospholipon® 90H [28, 50, 88]. The characteristic FT-IR signals exhibited by the PM are shown in (Fig. 6c). The signals appeared at 3367.86, 3202.94, 2957.00, 2917.46, 2849.95, 1725.10, 1649.21, 1623.17, 1253.78, 1095.61, and 589.28 cm^{-1}. The appearance of these peaks in the FT-IR spectrum indicated a strong alliance between pure MGN and Phospholipon 90H®. Finally, the MPLC FT-IR spectrum (Fig. 6d) showed the absorption signals at 3368.82, 3260.80, 3237.66, and 1623.17 cm^{-1}. In addition to this, no new extra peaks were seen. These signals were shifted from lower to higher frequencies specific to the functional groups O-H and C=O. The shifting of peaks in MPLC compared with pure MGN suggested that the presence of weak

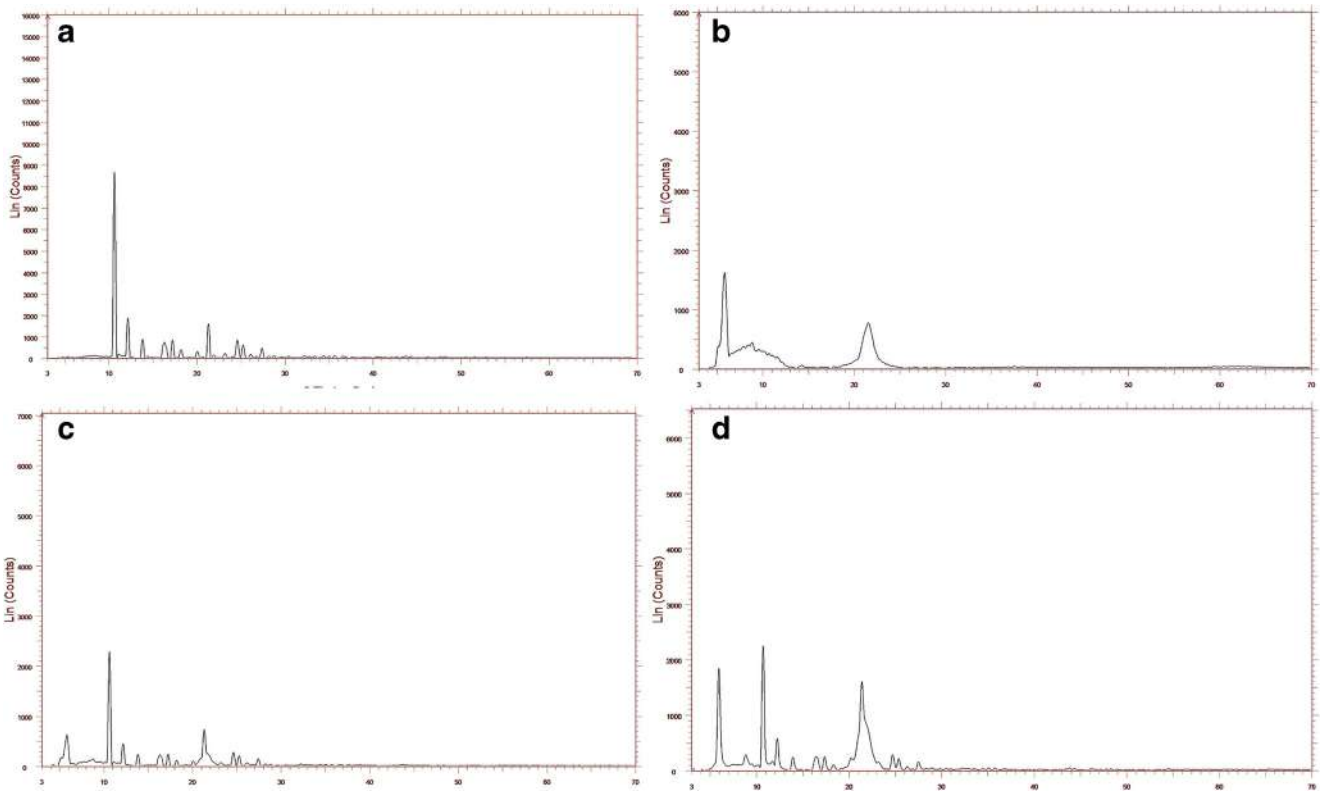

Fig. 7 The X-ray diffractograms of **a** pure MGN, **b** Phospholipon® 90H, **c** the physical mixture (1:1.76) of pure MGN and Phospholipon® 90H, and **d** MPLC formulations

intermolecular interactions, i.e., H-bonding, van der Waals forces, and/or ion-dipole forces, is involved in the formation of MPLC.

PXRD

The diffractograms for pure MGN, Phospholipon® 90H, PM, and the MPLC formulation are shown in Fig. 7a, b, c, and d, respectively. On the 2θ scale, multiple diffraction peaks were shown by pure MGN (Fig. 7a). Three sharp peaks were seen at 10^0, 12^0, and 21^0, and their intensity was found to be higher around ~ 8500, 2000, and 1000 counts on *y*-axis. Moreover, some additional low-intensity peaks appeared at 13.5^0, 16^0, 17^0, 18^0, 20^0, 24^0, 25^0, and 27^0. These peaks signified the crystalline nature of pure MGN [17]. The Phospholipon® 90H diffraction spectrum (Fig. 7b) exhibited two peaks. The first peak appeared at 5^0, while the second one was seen at 21^0. The intensities of these peaks were around ~ 1600 and 800 counts on the *y*-axis scale, respectively. Moreover, the absence of sharp and intense peaks in this diffractogram indicated its amorphous nature [29, 30, 48]. Abundant diffraction signals were displayed in diffractograms of the PM (Fig. 7c). These signals were seen at 5^0, 10^0, 12^0, 13^0, 16^0, 17^0, 18^0, 21^0, 22^0, and 23^0, indicating a partial interaction between MGN and Phospholipon 90H®. The intensity of the MGN peak in the physical mixture was lower around ~ 2100 and 500 counts on the *y*-axis, compared with the pure MGN, possibly indicating a lower fraction of pure MGN and hindrance of phospholipids and in situ formation of partial aggregates. It was evident that the PM exhibited a relatively different diffractogram compared with those of MGN and Phospholipon® 90H individually [47]. As depicted in (Fig. 7d), MPLC exhibited more or less similar diffraction pattern as that of the PM. However, the intensity of phospholipid-dominated peaks was increased, whereas the MGN-dominated peak intensity was suppressed around ~ 2350 and 600 counts on the *y*-axis. Moreover, the third intense peak of MGN disappeared completely in MPLC, which might be attributed to the merging of the third peak into the phospholipid-dominated peak. Therefore, based on the changes in peak intensities in MPLC compared with pure MGN, it could be ascertained that the complexation proceeded successfully, wherein the crystalline MGN dispersed into the phospholipid matrix resulting in the conversion of crystalline MGN to amorphous MPLC; the complex is stabilized by weak intermolecular interactions.

^{1}H-NMR

The ^{1}H-NMR spectra of pure MGN, Phospholipon® 90H, and optimized MPLC are recorded on the δ scale and their spectrums are depicted in Fig. 8 (a, b, c, and d), respectively. Pure MGN (Fig. 8a) exhibited chemical shift values around

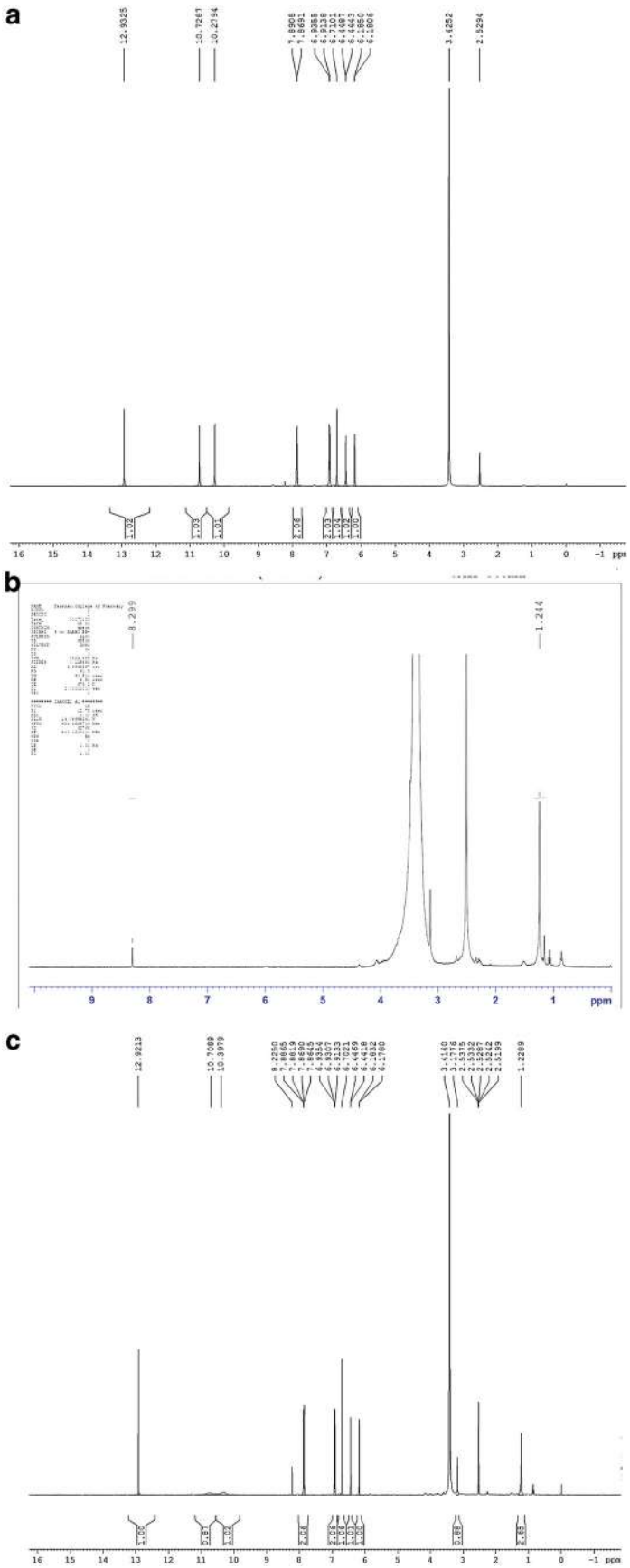

Fig. 8 1H-NMR spectra of **a** pure MGN, **b** Phospholipon® 90H, and **c** MPLC formulations

~ δ 12.93 (1H, s, 1-OH), δ10.73 (1H, s, 6-OH), δ10.28 (1H, s, 3-OH, and 7-OH), δ7.88 (1H, s, H-8), δ6.92 (1H, s, H-5), and δ6.44 (1H, s, H-4, and H-6). Results are consistent with earlier published literature [89]. Chemical shift values of Phospholipon®90 (Fig. 8b) appeared around ~ δ 4.85 (1H, s), δ 4.08–δ 3.96 (br s, 1H), δ 3.83–δ 3.62 (s, 2H), δ 3.38 (s, 1H), δ 3.07 (s, 15H), δ 2.95 (H-8, J = 8 Hz), δ 2.27 (s, 1H), δ 1.26 (s, 2H, s), δ 0.95 (s, 23H), and δ 0.57 (s, 3H, s) [90]. The ^{1}H-NMR spectrum of optimized MPLC formulation is shown in (Fig. 8c). It exhibited values around ~ δ12.92 (1H, s, 1-OH), δ 10.70 (1H, s, 6-OH), δ 10.39 (1H, s, 3-OH, and 7-OH), δ8.225 (2H), δ 7.88 (1H, s, H-8), δ6.93 (1H, s, H-5), δ6.44 (1H, s, H-4, and H-6), δ3.17 (s, 3H), and δ1.23 (s, 3H), respectively. Upon comparison, it was observed that there is a significant shifting of proton signals in downfield (δ > 7) and upfield (δ < 4) aromatic region of the MPLC, indicating the formation of a molecular complex between the specific phenolic (3-OH, 6-OH, and 1-OH) group of MGN with the polar head of Phospholipon® 90H through the involvement of hydrogen bonding, ion-dipole, and van der Waals forces of interaction (29, 48). This conclusion suggests the weak intermolecular forces are the main mechanism involved in the formation of stable MPLC.

Solubility studies

The results obtained from the solubility studies of pure MGN, MGN SNPs, PM, optimized MPLC, and MPLC SNPs formulation in water or n-octanol are shown in Table 4. It is seen that pure MGN and MGN SNPs possessed low aqueous solubility (0.34 and 0.37 μg/mL), while the observed solubility in n-octanol was 178- and 182-fold higher (60.78 and 64.20 μg/mL). It was not surprising given the BCS class IV status of MGN [91]. The outcome of PM solubility studies was a moderate increase (up to 10-fold) in aqueous solubility (3.41 μg/mL) over pure MGN. This observation was statistically significant ($p < 0.05$). In contrast to aqueous solubility, the PM did not show significant improvement in solubility in n-octanol. The considerable improvement in aqueous solubility of the PM was attributed to the close association of amphiphilic Phospholipon® 90H with pure MGN during the complexation process. Interestingly, the solubility of MPLC formulation in water increased significantly (10.79 μg/mL, ~ 32-fold) over pure MGN and the PM. Additionally, the solubility of MPLC formulation in n-octanol was observed to be 257.15 μg/mL. This was attributed to the physicochemical modification as well as the amorphization of pure MGN during complexation with amphiphilic Phospholipon® 90H. The MPLC SNPs showed a significant ($p < 0.001$) increase in aqueous solubility (13.39 μg/mL, ~ 39-fold) over pure MGN. From this comparative solubility analysis, it could be concluded that the MPLC SNPs significantly improved the aqueous solubility of MGN, and it was likely due to the amorphized and amphiphilic-assisted nanosized nature of MPLC SNPs.

Functional characterization of MPLC and MPLC SNPs

In vitro dissolution studies The comparative in vitro release pattern of pure MGN suspension, MGN SNPs, MPLC, and MPLC SNPs in PBS (pH 7.4) using dialysis method is shown in (Fig. 9). The dissolution pattern of MGN suspension and MGN SNPs exhibited ~ 27 and ~ 30% release (0–5 h) and ~ 41 and ~43% release at the end of 12 h. This could be due to poor aqueous solubility of MGN. These results correlated well with the solubility studies [91]. In comparison, both the MPLC and MPLC SNPs demonstrated a sharp enhancement in the rate and extent of dissolution of MGN. For the initial phase (0–5 h), the MPLC exhibited ~ 53% release, and subsequently, the MGN release increased significantly and reached ~ 85% at the end of the 12-h testing period. The increased MPLC dissolution was likely due to the increased solubility and wettability of MGN in MPLC owing to the complex formation with Phospholipon® 90H, resulting in uniform dispersion in the dissolution medium. These findings agreed with the earlier reports [48, 92]. The release profile of MGN from MPLC SNPs showed that the MGN displayed a burst release (~ 71%) in the initial phase (0–5 h). However, after 5 h, around ~ 98% of the sustained release of MGN was observed. The MPLC SNPs exhibited a more sustained release and it was indicated by the initial burst release and latter prolonged-release behavior. The initial burst release was attributed to the absorption of MPLC on the surface of soft nanoparticles that undergo dissociation of MGN and released in free form in

Table 4 Solubility analysis of pure MGN, MGN SNPs, the physical mixture (1:1.76) of MGN and Phospholipon® 90H (PM), design-optimized MPLC, and lyophilized MPLC SNPs

Samples	Aqueous solubility (μg/mL)*	n-octanol solubility (μg/mL)*
Pure MGN	0.34 ± 0.09	60.78 ± 0.21
MGN SNPs	0.37 ± 0.12	64.20 ± 0.36
PM	3.41 ± 0.17	67.42 ± 0.43
MPLC	10.79 ± 0.32	109.08 ± 0.20
MPLC SNPs	13.39 ± 0.22	117.20 ± 0.44

*Data are represented as mean ± SD ($n = 3$)

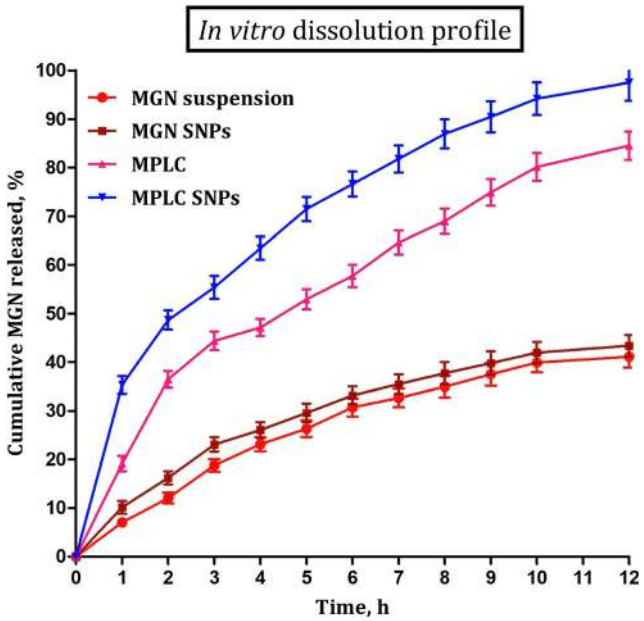

Fig. 9 The in vitro dissolution profiles of MGN release from MGN suspension, MGN SNPs, prepared MPLC, and MPLC SNPs formulations. Values are presented as mean ± Std. Dev. ($n = 3$)

dissolution medium, whereas prolonged-release was attributed to the presence of stabilized MPLC within the core space of soft nanoparticles, and from this, the MGN showed diffusion-controlled sustained release via two stages: firstly, the MGN dissociated from MPLC, and secondly, the dissociated MGN within the core space diffused through the skeleton of soft nanoparticles. These outcomes indicate that MGN is stable and release in a sustained manner for a long period attributed to the formation of MPLC and following its incorporation into SNPs. Results are well supported by previous reports [45]. The comparative release profile indicated that MPLC SNPs provided a sustained release of MGN for longer periods, compared with that of MPLC and suspension. This only

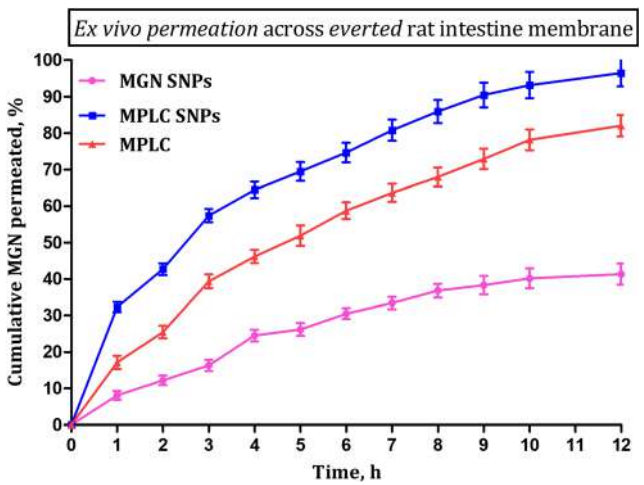

Fig. 10 Ex vivo permeation profiles of MGN permeated from MGN SNPs, MPLC, and prepared MPLC SNPs across *everted* rat intestine membrane. Values are presented as mean ± Std. Dev. ($n = 3$)

emphasized that MPLC SNPs could be an effective nanovesicle drug delivery system for the oral administration of MGN.

The release kinetics of MGN from the formulation was estimated by the fitting of the observed release data into various kinetic models, i.e., first-order, zero-order, Higuchi, and Korsmeyer-Peppas models [93]. The MPLC-loaded SNPs exhibited correlation coefficient value ($R^2 = 0.983$). Based on this result, the Higuchi model was found to be the best-fit kinetic model, which described the underlying dissolution mechanism. Moreover, the same formulation ($n = 0.49$) indicated that the MPLC SNPs followed diffusion as the main mechanism for MGN release. It is essentially described as a two-step process—(i) MGN was released from MPLC and (ii) free MGN then diffused through the phytosomal matrix into the surrounding medium.

Ex vivo permeability studies The permeability of pure MGN from MGN SNPs, MPLC, and MPLC SNPs formulations across the everted rat intestine membrane was studied using a specially designed apparatus, and the generated results are depicted in (Fig. 10). At the end of the 12-h permeation period, MGN from MGN SNPs exhibited only ~41% of permeation across the everted rat intestinal membrane. This was likely due to the low permeability of MGN following the earlier reports. Compared with the MGN SNPs, the MPLC and MPLC SNPs showed a higher rate and extent of permeation across the intestinal membrane. By the end of the 12-h permeation period, the MPLC demonstrated around ~82% of MGN permeation, whereas the MPLC SNP formulation demonstrated ~97% of MGN permeation. The results are correlated with dissolution studies.

The observed difference in permeation studies could be attributed to the formulation methods and phospholipids. In this study, the MPLC and MPLC SNPs were prepared from the same phospholipids, and as reported earlier, the phospholipids on complexation with bioactive improved its permeability via increasing the amphiphilic nature of bioactive. Moreover, the similarity of the structural component of employed phospholipids with the lipid content of mammalian cell membrane exhibits biocompatibility toward each other [94]. The biological cell membrane is also made up of phospholipid bilayer and shows the amphiphilic character (the fluid mosaic model proposed by S. J Singer and G. L. Nicolson in 1972). So it may be assumed that the improved amphiphilicity of MGN using the Phospholipon® 90H could show higher miscibility with the biological cell membrane and facilitate effective permeation of MGN [72]. The soft nanoparticles, i.e., MPLC SNPs, prepared using a combination of solvent evaporation and nanoprecipitation method have modified the MGN physicochemically, resulting in an increase of lipophilicity followed by permeation. According to previous studies, it has been reported that the nanoparticles prepared

using phospholipids increase their affinity toward the biological cell membrane and maximize the drug permeation [95–97]. In MPLC SNPs, the presence of the excess amount of MPLC as well as amphiphilic nature of soft nanoparticles could also increase strong affinity toward the cell membrane and allow greater miscibility within the phospholipid bilayer of the cell membrane, significantly enhancing the permeability of MPLC SNPs compared with MPLC and MGN. Moreover, the affinity of MPLC SNPs toward the plasma membrane provides strong interaction between them, which may cause destabilization of the membrane as well as the formation of pore within the membrane, resulting in the translocation and permeation of nanoparticles via exchanging of coating lipids between MPLC SNPs and lipid bilayer [98]. Additionally, the adhesion (i.e., partial wrapping) and complete wrapping and internalization of MPLC SNPs within the plasma membrane and, subsequently, membrane pore formation may also be answerable for the enhancement of MGN permeation [99]. The permeation study indicated that MPLC enhances the permeation of MGN, but in the form of soft nanoparticles, their strong affinity to the cell membrane as well as lipid exchange mechanism could enhance their permeation to a greater extent and subsequently increase the oral bioavailability of MGN.

In vivo antioxidant activity The influence of orally administrated formulations containing MGN on CCl_4-induced albino rats is discussed below.

Liver function test

The damage to the hepatic tissue in all groups of animals was induced by a well-known hepatotoxin, CCl_4. After oral administration, the CCl_4 was metabolized to reactive oxygen species (ROS), i.e., free radicals, mediated via CYP450 enzymes. The generated ROS further biochemically reacted with various biological macromolecules such as lipids, proteins, and carbohydrates, which in turn led to oxidative damage.

Table 5 lists the results obtained from the antioxidant studies of MGN SNPs suspension and MPLC SNPs on liver function tests. The marker enzymes such as SGOT, SGPT, total bilirubin, and SALP were elevated significantly following induction by CCl_4. However, this elevation in the marker enzymes was restored by the administration of antioxidant formulations to the animals. The MGN SNPs suspension (dose: 60 mg/kg, p.o.) exhibited a significant ($p < 0.05$) reduction in SGOT, SGPT, total bilirubin, and SALP. In contrast to this, the MPLC SNPs demonstrated a more significant ($p < 0.01$) reduction in the marker enzymes at the same dose level. In conclusion, the MPLC SNPs exhibited a significant hepatoprotective activity, compared with the MGN SNPs suspension.

In vivo antioxidant marker enzyme estimation

The performance of orally administrated formulations containing MGN on the in vivo antioxidant marker enzymes such as GSH, SOD, CAT, and LPO in CCl_4-induced albino rats is shown in (Fig. 11). After CCl_4 administration, the GSH level in rat liver homogenate was reduced rapidly compared with the normal group. In contrast, the MGN SNP-treated animals (dose: 60 mg/kg, p.o.) significantly ($p < 0.05$) increased the GSH levels. Compared with the MGN SNP suspension, a more significant ($p < 0.01$) enhancement in the GSH level was produced by the MPLC SNPs at the same dose level. Reduction in the SOD level was observed compared to the positive control. The MGN SNPs suspension increased the SOD significantly *($p < 0.05$)* at the dose level of (~ 60 mg/kg, p.o.). The MPLC SNPs (dose: 60 mg/kg of MGN, p.o.) showed an improvement ($p < 0.01$) in SOD levels, compared to the MGN SNPs. Reduction in the CAT level in the rat liver homogenate was observed following the oral administration of CCl_4. A significant ($p < 0.05$) increase in the CAT level was

Table 5 Effect of MGN SNPs and lyophilized MPLC SNPs on CCl_4-intoxicated liver function marker enzymes, SGOT, SGPT, SALP, and total bilirubin

Treatment groups	SGPT (IU/L)[a]	SGOT (IU/L)[a]	SALP (IU/L)[a]	Total bilirubin (mg/dL)
Group I: Normal [Tween® 20 (1%, v/v, p.o.)]	28.03 ± 1.06**	31.10 ± 1.22**	144.31 ± 2.18**	0.30 ± 0.06**
Group II: Control [CCl_4 and olive oil (1:1, 5 mL/kg, i.p.)]	61.27 ± 2.02	79.42 ± 3.51	187.34 ± 4.08	0.87 ± 0.03
Group III: MGN SNPs (~ 60 mg/kg, p.o.) [CCl_4 and olive oil (1:1, 5 mL/kg, i.p. for 7 days)]	50.14 ± 2.30*	64.19 ± 1.86*	175.49 ± 2.39*	0.67 ± 0.09*
Group IV: MPLC SNPs (~ 60 mg/kg of MGN, p.o.) [CCl_4 and olive oil (1:1, 5 mL/kg, i.p. for 7 days)]	34.54 ± 1.17**	42.28 ± 1.60**	151.20 ± 2.59**	0.46 ± 0.08**

[a] *IU/L* International Units/Liter of plasma

All values are Mean ± Std. Error of Mean ($n = 6$)

*$p < 0.05$, **$p < 0.01$ (significant with respect to control group)

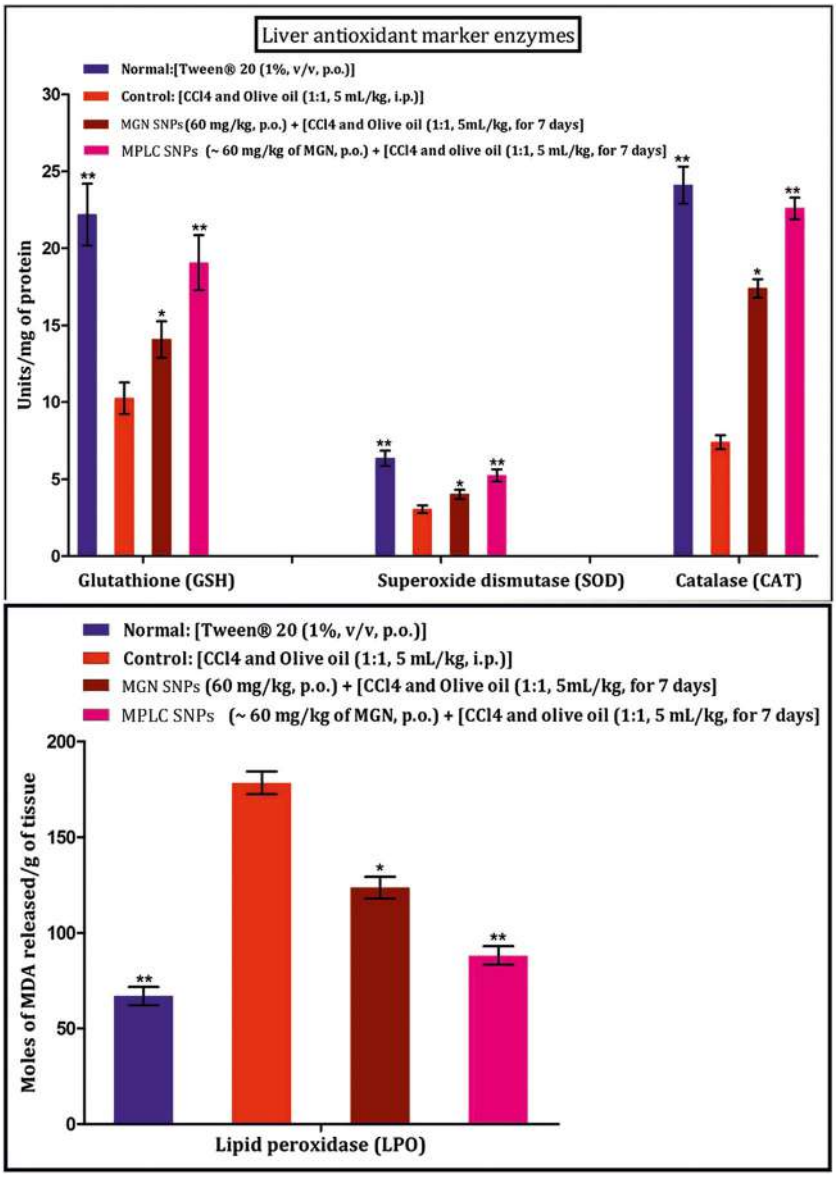

Fig. 11 Effect of MGN SNPs and MPLC SNPs on rat liver antioxidant marker enzymes, such as glutathione reductase (GSH) (nmoles/mg of protein), superoxide dismutase (SOD) (units/mg protein), catalase (CAT) (units/mg protein), and lipid peroxidase (LPO) (nmoles of MDA released/g tissue). Values are Mean ± Std. Error of Mean ($n = 6$). *$p < 0.05$, **$p < 0.01$ (significant with respect to control groups)

recorded in the case of pure MGN SNP suspension at a dose of ~ 60 mg/kg, p.o. A further increase in the CAT level in liver homogenate was seen more significantly ($p < 0.01$) after oral administration of MPLC SNPs at the same dose level. In the case of LPO, the MGN SNP suspension lowered its level ($p < 0.05$) in liver homogenate at (~ 60 mg/kg, p.o.) dosing. The MPLC SNP-treated animals at a dose of ~ 60 mg/kg of MGN, p.o. exhibited higher and significant ($p < 0.01$) elevation in the LPO levels in rat liver homogenate. The overall study indicated that MPLC SNPs provide more significant hepatoprotection against CCl_4 intoxication. CCl_4 is a well-known causative agent for the liver. Following administration, CCl_4 metabolized into trichloromethyl radical [100], which causes an increase in lipid peroxidation and lowering of some enzyme functionality [101], resulting in the production of hepatocellular degeneration and centrilobular necrosis in the liver [102, 103]. Earlier reports have shown that numerous bioactive compounds produce a significant antioxidant activity against CCl_4 -induced hepatotoxicity. MGN, a xanthone compound, also produces an antioxidant activity against CCl_4-induced liver damage. Moreover; it is also reported as a potent free radical scavenger, which scavenges the free radical and, subsequently, protects the liver [4]. However, poor bioavailability, poor absorption, and low lipophilicity of MGN limited its antioxidant activity. In this study, the above major issue of MGN was solved by converting it into soft nanoparticles loaded with MPLC and evaluated its activity against MGN SNPs. The MGN SNPs are soft nanoparticles loaded with MGN without complex that still showed significant results in liver function test and in vivo antioxidant studies attributed to slight improvements in aqueous as well as lipid solubility and its results are reflected in Table 4.

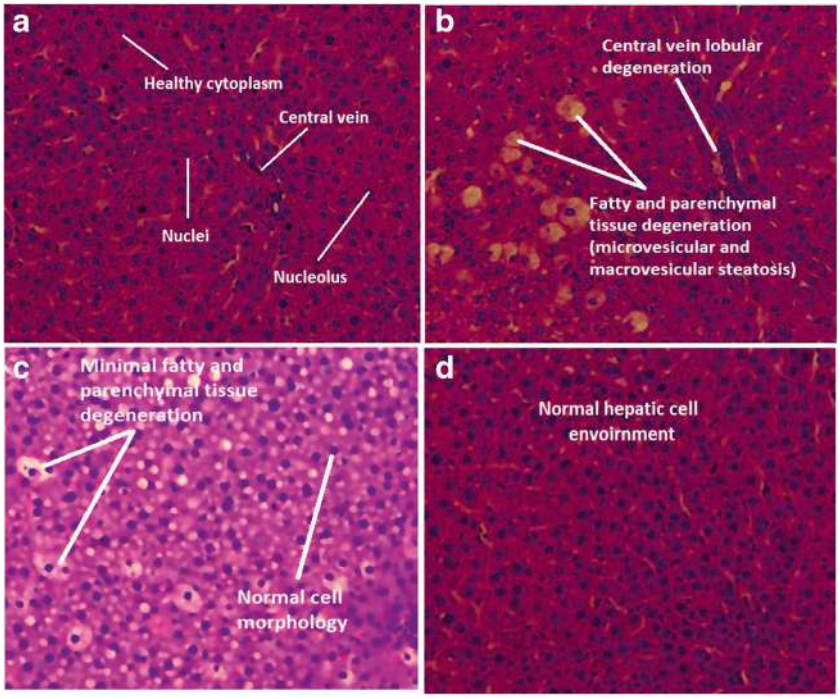

Fig. 12 Histopathology micrographs of (× 400) of rat livers. **a** Normal: Tween® 20 (1%, *v*/v, p.o.), **b** control: CCl_4 + olive oil (1:1, 5 mL/kg, i.p), **c** MGN SNPs (60 mg/kg, p.o.) + [CCl_4 + olive oil (1:1, 5 mL/kg, i.p. for 7 days], and **d** MPLC SNPs (~ 60 mg/kg of MGN, p.o.) + [CCl_4 + olive oil (1:1, 5 mL/kg, i.p. for 7 days]

Compared with MGN SNPs, the MPLC SNPs show more significant effects. The positive results of MPLC SNPs were attributed to the following factors that may be involved. First, the affinity of MPLC SNPs toward the plasma membrane can provide complete wrapping, internalization, and formation of the pore of nanoparticles within the membrane, resulting in the enhancement of permeation of MGN and, thus, increasing the in vivo antioxidant activity. Second, the lipid exchange mechanism between coating lipids of MPLC SNPs and bilayer may enhance the translocation and permeation of MGN into hepatic cells leading to the increase of antioxidant enzyme levels. Third, the improved biological half-life of MGN by converting into MPLC SNPs also increases its effective time in systemic circulation, resulting in more utilization of MGN by damaged hepatic cells. Forth, the sustained release characteristics of MPLC SNPs may provide a prolonged exposure of the damaged hepatic cells to MGN, leading to the enhancement of the hepatoprotection against CCl_4. Finally, the improved lipophilicity of MPLC SNPs can increase its miscibility with lipid content of biological membrane; facilitate its effective transportation across the membrane, subsequently, entering the hepatic cells; and show an effective antioxidant

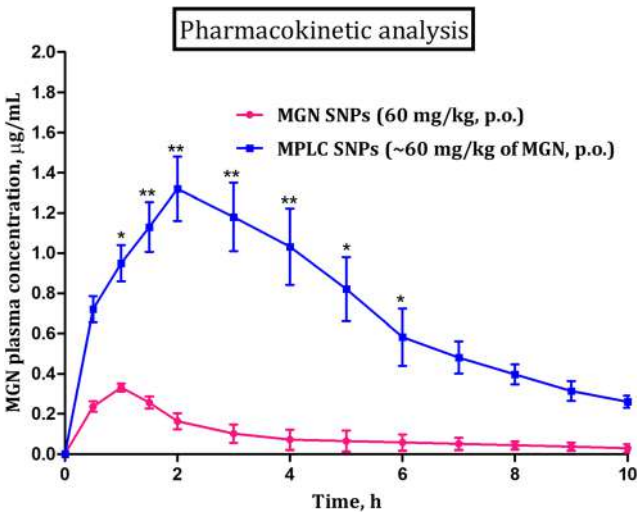

Fig. 13 Mean plasma concentration time profile curve after oral administration of MGN SNPs (60 mg/kg, p.o.) and MPLC SNPs (~ 60 mg/kg of MGN, p.o.). Values are mean ± Std. Error of Mean. (n = 6). *$p < 0.05$ and **$p < 0.01$ (significant with respect to MGN SNPs-treated group)

Table 6 Pharmacokinetic parameters for group of animals after oral administration of MGN SNPs (60 mg/kg, p.o.) or MPLC SNPs (~ 60 mg/kg of MGN, p.o.)

Pharmacokinetic parameters	Treatment	
	MGN SNPs	MPLC SNPs
C_{max} (µg mL^{-1})	0.33 ± 0.10	1.32 ± 0.40
T_{max} (h)	1.00 ± 0.31	2.00 ± 0.19
$AUC_{0\text{-}t}$ (µg h mL^{-1})	0.74 ± 0.07	7.11 ± 1.43
$AUC_{0\text{-}\infty}$ (µg h mL^{-1})	0.96 ± 0.58	7.30 ± 1.65
$t_{1/2el}$ (h)	2.82 ± 1.29	3.22 ± 1.04
K_{el} (h^{-1})	0.39 ± 0.04	0.19 ± 0.09
cl/F [(mg)/µg mL^{-1} h^{-1})]	74.22 ± 2.41	9.39 ± 1.71
Vz/F (L/kg)	302.41 ± 1.28	43.64 ± 2.45
Relative bioavailability (F)	–	53.29

All values are Mean ± Std. Error of Mean (n = 6)

Table 7 Stability studies of lyophilized MPLC SNPs at 4 and 25 °C

Parameters	At 4 °C			At 25 °C	
	0 months	3 months	6 months	3 months	6 months
Particle size (nm)	906.69 ± 0.20	910.18 ± 2.10	915.08 ± 1.18	920.21 ± 2.34	931.28 ± 2.46
PDI	0.50 ± 0.19	0.56 ± 0.04	0.61 ± 0.19	0.65 ± 0.39	0.73 ± 0.11
Zeta potential (mV)	−12.22 ± 0.33	−14.05 ± 1.49	−15.56 ± 2.65	−16.21 ± 1.388	−20.43 ± 1.05
Entrapment efficiency (%)	81.63 ± 0.41	79.86 ± 1.41	77.91 ± 2.10	76.66 ± 1.54	67.58 ± 1.77

All values are mean ± SD ($n = 3$)

activity. So, this study suggested that MPLC SNPs could be a promising delivery system in the enhancement of the in vivo antioxidant activity of MGN compared with MGN SNPs.

Histopathological studies

The investigations of CCl_4-induced liver damage of rats in hematoxylin-eosin-stained microscopic (× 400) images from groups of animals treated with vehicle (Tween® 20), CCl_4 only, CCl_4 and MGN SNP suspension, and CCl_4 and MPLC SNPs are shown in Fig. 12 (a, b, c, and d), respectively. As seen in (Fig. 12a), there were no gross pathological changes in the vehicle-treated animals. In sharp contrast, the CCl_4-treated animals (Fig. 12b) exhibited pathological changes such as damage to the fat (steatosis) as well as parenchymal cells. Additionally, CCl_4 also damaged the central lobular vein extensively. Animals treated with MGN SNP suspension (Fig. 12c) demonstrated a significant hepatoprotective activity with modest tissue recovery. Compared with MGN SNPs, the MPLC SNPs (Fig. 12d) demonstrated a highly significant recovery to the damaged hepatic tissue by protecting for longer periods. These results confirmed that the MPLC SNPs offered a significant hepatoprotection to the CCl_4-exposed hepatic cells, likely due to the nanosized nature of the drug delivery system.

HPLC method validation

The results obtained from the HPLC method validation studies are discussed below. The concentration range (0.05–10 μg/mL) showed good linear relation between the selected concentration range and correlation coefficient ($r^2 = 0.9970$). The results of the limit of detection and limit of quantification appeared around ~ 10 and 32 ng/mL, respectively. The results of intra-day and inter-day precision were found to be within the value of ~ 4%. The absolute extraction recoveries of MGN from rat plasma samples were observed to be in the range of ~ 95.2–96.6%, respectively. After freeze-thaw cycles, the MGN demonstrated excellent stability, and the variation content of MGN was found to be ~ 8%. At the end of short-term and long-term stability studies, the MGN appeared to be stable. The variation of MGN content was found to be ~ 7 and 16%, respectively.

Pharmacokinetic analysis

The mean plasma concentration time profile obtained following oral administration of MGN SNPs (60 mg/kg, p.o.) or MPLC SNPs (60 mg/kg of MGN, p.o.) to a group of animals is shown in (Fig. 13). The MGN SNPs displayed C_{max} (0.3 μg/mL) within 1 h, following which there was a consistent decrease in mean plasma concentration up to 10 h. In contrast to this, the MPLC SNPs demonstrated C_{max} (0.95 μg/mL) within 1 h. The MGN concentration further increased to 1.3 μg/mL at 2 h. However, beyond this period, the MGN plasma concentration decreased at a much slower rate up to 10 h. From this observation, it is clear that the MPLC SNPs increased the MGN plasma concentration to a great extent, compared with the MGN SNPs. This observation validated our original objective of improving the biopharmaceutical profile of MGN significantly.

The obtained pharmacokinetic data were analyzed using the WinNonlin® (Version 4.1, Certara USA Inc., Princeton, NJ, USA) software. The detailed analyses are shown in Table 6. The orally administrated MPLC SNPs (dose: 60 mg/kg of MGN, p.o.) displayed a higher C_{max} (1.32 μg/mL), T_{max} (2.0 h), and $AUC_{0\text{-}\infty}$ (7.3 μg mL^{-1} h) compared with the MGN SNPs. Likewise, the elimination half-life value ($t_{1/2el}$) was also found to be higher around 3.22 h for MPLC SNPs compared with MGN SNPs. Moreover, the clearance (Cl/F), elimination rate constant (K_{el}), and volume of distribution (Vz/F) for MPLC SNPs were found to be lowered around 9.39 μg mL^{-1} h^{-1}, 0.191 h^{-1}, and 43.64 L, respectively, compared with the MGN SNPs. The calculated bioavailability value (F) for MPLC SNPs was 53.29%. Based on the differences in pharmacokinetic parameters for both formulations, it indicates that MPLC SNPs significantly modified the MGN due to complexation with Phospholipon® 90H along with the nanoformulation.

Stability studies

The results of long-term stability studies are shown in Table 7. As seen in the table, the MPLC SNPs at both temperature of 25 and 4 °C demonstrated no significant change in the particle size, PDI, zeta potential, and entrapment efficiency of final formulation, indicating the presence of sucrose at 2% *w*/*w* as a cryoprotectant in lyophilized formulation could enhance the stability of the formulation. This result also suggested that the molecularly interacted MGN with the polar head of Phospholipon® 90H in lyophilized MPLC SNPs formulations could increase their affinity toward each other as well as the lipophilicity of MPLC, thus, enhancing the stability of MPLC SNPs.

Conclusions

The developed self-assembled MPLC SNPs using a combination of solvent evaporation and nanoprecipitation method significantly improved the aqueous solubility, in vitro dissolution rate, oral bioavailability, and in vivo antioxidant potential of MGN. The characterization studies confirmed the formation of MPLC and MPLC SNPs through the contribution of weak intermolecular forces of interactions, such as H-bonding, ion-dipole forces, van der Waals forces, etc., between the polar parts of MGN and the Phospholipon® 90H. The MPLC SNPs exhibited a smaller particle size and favorable zeta potential, indicating its suitability for oral administration. Overall, the MPLC and MPLC SNPs drastically enhanced the aqueous solubility (~ 32-fold and ~ 39-fold) of MGN compared with the MGN SNPs. The results of the in vitro dissolution studies showed that MPLC SNPs significantly enhanced the rate and extent of MGN release via burst and then sustained release about ~ 98% at the end of the 12-h dissolution testing, over to that of MGN SNPs. The MPLC SNPs exhibited a higher rate and extent of permeation around ~ 97%, compared with the MGN SNPs. The in vivo antioxidant potential of MPLC SNPs was enhanced significantly ($p < 0.001$) in the CCl_4-induced hepatotoxicity in rats when compared with the MGN SNPs. Moreover, the MPLC SNPs (dose: 60 mg/kg of MGN, p.o.) improved the oral bioavailability considerably over MGN SNPs. The final formulation demonstrated an excellent antioxidant potential in vivo by offering significant restoration of the hepatic cellular microenvironment. Overall, the promising results evidenced that the developed self-assembled MPLC SNPs offered an effective nanovesicle delivery system for enhancing the biopharmaceutical and in vivo antioxidant potential of MGN.

Acknowledgments The corresponding author is thankful to Dr. Milind J. Umekar, Principal, Smt. Kishoritai Bhoyar College of Pharmacy, New Kamptee, Nagpur, for providing instrument facilities to complete this research work. The author is also thankful to Dr. Shirish P. Jain, Principal, Rajarshi Shahu College of Pharmacy, Buldhana, for constant financial and technical support to complete this manuscript on time.

Author contribution Darshan Telange: conceptualization, investigation, methodology, writing of the original draft, writing the review, and editing
Nazish Sohail: methodology, investigation, and data curation
Atul Hemke: validation and data curation
Prashant Kharkar: investigation, methodology, and writing of the original draft
Anil Pethe: conceptualization, supervision, investigation, and visualization

Funding information The current research work did not receive any funding from government agencies.

Compliance with ethical standards

Conflict of interest The authors declared that they have no conflict of interest.

Ethical approval The Institutional Animal Ethical Committee (IAEC) of Smt. Kishoritai Bhoyar College of Pharmacy, New Kamptee, Nagpur, sanctioned and approved the experimental protocols (*SKBCOP/IAEC/2017–2018, dated August 13, 2018*) for the current study. The studies were carried out according to the ethical guidelines available by the Committee for Purpose of Control and Supervision of Experiments on Animals (CPCSEA).

References

1. Yoshimi N, Matsunaga K, Katayama M, Yamada Y, Kuno T, Qiao Z, et al. The inhibitory effects of mangiferin, a naturally occurring glucosyl xanthone, in bowel carcinogenesis of male F344 rats. Cancer Lett. 2001;163(2):163–70. https://doi.org/10.1016/s0304-3835(00)00678-9.
2. Yoshikawa M, Ninomiya K, Shimoda H, Nishida N, Matsuda H. Hepatoprotective and antioxidative properties of Salacia reticulata: preventive effects of phenolic constituents on CCl4-induced liver injury in mice. Biol Pharm Bull. 2002;25:72–6. https://doi.org/10.1248/bpb.25.72.
3. Das J, Ghosh J, Roy A, Sil PC. Mangiferin exerts hepatoprotective activity against D-galactosamine induced acute toxicity and oxidative/nitrosative stress via Nrf2-NFκB pathways. Toxicol Appl Pharmacol. 2012;260:35–47. https://doi.org/10.1016/j.taap.2012.01.015.
4. Imran M, Arshad MS, Butt MS, Kwon JH, Arshad MU, Sultan MT. Mangiferin: a natural miracle bioactive compound against lifestyle-related disorders. Lipids Health Dis. 2017;16:1–17. https://doi.org/10.1186/s12944-017-0449-y.
5. Moreira RRD, Carlos IZ, Vilegas W. Release of intermediate reactive hydrogen peroxide by macrophage cells activated by natural products. Biol Pharm Bull. 2002;24:201–4. https://doi.org/10.1248/bpb.24.201.
6. Ghosh J, Das J, Manna P, Sil PC. The protective role of arjunolic acid against doxorubicin-induced intracellular ROS dependent JNK-p38 and p53-mediated cardiac apoptosis. Biomaterials. 2011;32:4857–66. https://doi.org/10.1016/j.biomaterials.2011.03.048.
7. Rodeiro I, Delgado R, Garrido G. Effects of a *Mangifera indica* L. stem bark extract and mangiferin on radiation-induced DNA damage in human lymphocytes and lymphoblastoid cells. Cell Prolif. 2014;47:48–55. https://doi.org/10.1111/cpr.12078.

8. Na L, Zhang Q, Jiang S, Shanshan D, Zhang W, Li Y, et al. Mangiferin supplementation improves serum lipid profiles in overweight patients with hyperlipidemia: a double-blind randomized controlled trial. Sci Rep. 2015;5:1–9. https://doi.org/10.1038/srep10344.
9. Henca I, Kokotkiewiczb A, Łuczkiewiczc P, Bryla E, Łuczkiewiczb M, Witkowskid JM. Naturally occurring xanthone and benzophenone derivatives exert significant anti-proliferative and proapoptotic effects in vitro on synovial fibroblasts and macrophages from rheumatoid arthritis patients. Int Immunopharmacol. 2017;49:148–54. https://doi.org/10.1016/j.intimp.2017.05.034.
10. Gelabert-Rebato M, Wiebe JC, Martin-Rincon M, et al. *Mangifera indica* l. leaf extract in combination with luteolin or quercetin enhances vo2peak and peak power output and preserves skeletal muscle function during ischemia-reperfusion in humans. Front Physiol. 2018;9:1–15. https://doi.org/10.3389/fphys.2018.00740.
11. Gelabert-Rebato M, Wiebe JC, Martin-Rincon M, Galvan-Alvarez V, Curtelin D, Perez-Valera M, et al. Enhancement of exercise performance by 48 hours, and 15-day supplementation with mangiferin and luteolin in men. Nutrients. 2019;11:2–24. https://doi.org/10.3390/nu11020344.
12. Yang Z, Weian C, Susu H, Hamim W. Protective effects of mangiferin on cerebral ischemia-reperfusion injury and its mechanism. Eur J Pharmacol. 2015;771:145–51. https://doi.org/10.1016/j.ejphar.2015.12.003.
13. Bhatt L, Sebastian B, Joshi V. Mangiferin protects rat myocardial tissue against cyclophosphamide-induced cardiotoxicity. J Ayurveda Integr Med. 2017;8(2):62–7. https://doi.org/10.1016/j.jaim.2017.04.006.
14. Szandurk M, Mervid-Lad A, Szelag A. The impact of mangiferin from belamcanda chinensis on experimental colitis in rats. Inflammopharmacology. 2018;26(2):571–81. https://doi.org/10.1016/j.jaim.2017.04.006.
15. Sahu AK, Verma VK, Mutneja E, Malik S, Nag TC, Dinda AK, et al. Mangiferin attenuates cisplatin-induced acute kidney injury in rats mediating modulation of MAPK pathway. Mol Cell Biochem. 2019;452(1–2):141–52. https://doi.org/10.1007/s11010-018-3420-y.
16. Basheer L, Kerem Z. Interactions between CYP3A4 and dietary polyphenols. Oxidative Med Cell Longev. 2015;2015:1–15. https://doi.org/10.1155/2015/854015.
17. Khurana RK, Bansal AK, Beg S, Burrow AJ, Katare OP, Singh KK, et al. Enhancing biopharmaceutical attributes of phospholipid complex-loaded nanostructured lipidic carriers of mangiferin: systematic development, characterization, and evaluation. Int J Pharm. 2017;518:289–306. https://doi.org/10.1016/j.ijpharm.2016.12.044.
18. Khurana RK, Gaspar BL, Welsby G, Katare OP, Singh KK, Singh B. Improving the biopharmaceutical attributes of mangiferin using vitamin E-TPGS co-loaded self-assembled phospholipid nano-mixed micellar systems. Drug Deliv Transl Res. 2018;8:617–32. https://doi.org/10.1007/s13346-018-0498-4.
19. Bhattacharyya S, Majhi S, Saha BP, Mukherjee PK. Chlorogenic acid – phospholipid complex improve protection against UVA-induced oxidative stress. J Photochem Photobiol B Biol. 2014;130:293–8. https://doi.org/10.1016/j.jphotobiol.2013.11.020.
20. Wang Q, Yang J, Cui W, Chen L, Lv F, Wen X, et al. Pharmacokinetic study of major bioactive components in rats after oral administration of extract of Ilex hainanensis by high-performance liquid chromatography/electrospray ionization mass spectrometry. J Pharm Biomed Anal. 2013;77:21–8. https://doi.org/10.1016/j.jpba.2013.01.011.
21. Ferreira F d R, Valentim IB, Ramones ELC, Trevisan MTS, Olea-Azar C, Perez-Cruz F, et al. Antioxidant activity of the mangiferin inclusion complex with β-cyclodextrin. LWT Food Sci Technol. 2013;51:129–34. https://doi.org/10.1016/j.lwt.2012.09.032.
22. Yang X, Zhao Y, Chen Y, Liao X, Gao C, Xiao D, et al. Host-guest inclusion system of mangiferin with β-cyclodextrin and its derivatives. Mater Sci Eng C Mater Biol Appl. 2013;33:2386–91. https://doi.org/10.1016/j.msec.2013.02.002.
23. Wang C, Jiang JD, Wu W, Kong WJ. The compound of mangiferin-berberine salt has potent activities in modulating lipid and glucose metabolisms in HepG2 cells. Biomed Res Int. 2016;2016:1–14. https://doi.org/10.1155/2016/8753436.
24. Liu R, Liu Z, Zhang C, Zhang B. Nanostructured lipid carriers as a novel ophthalmic delivery system for mangiferin: improving in vivo ocular bioavailability. J Pharm Sci. 2012;101(10):3833–44. https://doi.org/10.1002/jps.23251.
25. de Souza JRR, Feitosa JPA, Ricardo NMPS, Trevisan MTS, de Paula HCB, Ulrich CM, et al. Spray-drying encapsulation of mangiferin using natural polymers. Food Hydrocoll. 2013;33:10–8. https://doi.org/10.1016/j.foodhyd.2013.02.017.
26. Zhou Y, Dong W, Ye J, Hao H, Zhou J, Wang R, et al. A novel matrix dispersion based on phospholipid complex for improving oral bioavailability of baicalein: preparation, in vitro and in vivo evaluations. Drug Deliv. 2017;24:720–8. https://doi.org/10.1080/10717544.2017.1311968.
27. Zhang Z, Huang Y, Gao F, Bu H, Gu W, Li Y. Daidzein-phospholipid complex loaded lipid nanocarriers improved oral absorption: in vitro characteristics and in vivo behavior in rats. Nanoscale. 2011;3:1780–7. https://doi.org/10.1039/c0nr00879f.
28. Zhang WL, Cui Y, Fan Y-Q, Yang J-K, Liu P, Liu J-P, et al. Bioavailability, and foam cells permeability enhancement of salvianolic acid B pellets based on drug–phospholipids complex technique. Eur J Pharm Biopharm. 2012;83:76–86. https://doi.org/10.1016/j.ejpb.2012.09.021.
29. Telange DR, Patil AT, Pethe AM, Tatode AA, Anand S, Dave VS. Kaempferol-phospholipid complex: formulation, and evaluation of improved solubility, in vivo bioavailability, and antioxidant potential of kaempferol. J Excipients Food Chem. 2016;7(4):89–120.
30. Telange DR, Patil AT, Pethe AM, Fegade H, Anand S, Dave VS. Formulation and characterization of an apigenin-phospholipid phytosome (APLC) for improved solubility, in vivo bioavailability, and antioxidant potential. Eur J Pharm Sci. 2017;108:36–49. https://doi.org/10.1016/j.ejps.2016.12.009.
31. Citernesi U, Sciacchitano M. Phospholipids/active ingredient complexes. Cosm Toil. 1995;110:57–68.
32. Bhattacharya S. Phytosomes: emerging strategy in the delivery of herbal drugs and nutraceuticals. Pharma Times. 2009;41:9–12.
33. Fahy E, Subramaniam S, Brown HA. A comprehensive classification system for lipids. J Lipid Res. 2005;46:839–61. https://doi.org/10.1194/jlr.E400004-JLR200.
34. Renukuntla J, Vadlapudi AD, Patel A, Boddu SHS, Mitra AK. Approaches for enhancing oral bioavailability of peptides and proteins. Int J Pharm. 2013;447:75–93. https://doi.org/10.1016/j.ijpharm.2013.02.030.
35. Constantinides PP, Chaubal MV, Shorr R. Advances in lipid nanodispersions for parenteral drug delivery and targeting. Adv Drug Deliv Rev. 2008;60(6):757–67. https://doi.org/10.1016/j.addr.2007.10.013.
36. Kidd PM. Bioavailability and activity of phytosome complexes from botanical polyphenols: the silymarin, curcumin, green tea, and grape seed extracts. Altern Med Rev. 2009;14(3):226–46.
37. L. Bildstein, C. Dubernet, P. Couvreur, Prodrug-based intracellular delivery of anticancer agents. Adv. Drug Delivery Rev. 63 (1–2)(2011) 3–23. doi: https://doi.org/10.1016/j.addr.2010.12.005.
38. Bombardelli E. Phytosome: new cosmetic delivery system. Boll Chim Farm. 1991;130(11):431–8.

39. Peer D, Karp J, Hong S, et al. Nanocarriers as an emerging platform for cancer therapy. Nat Nanotech. 2007;2:751–60. https://doi.org/10.1038/nnano.2007.387.
40. Soussan E, Cassel S, Blanzat M, Rico-Lattes I. Drug delivery by soft matter: matrix and vesicular carriers. Angew Chem Int Ed. 2009;48(2):274–88. https://doi.org/10.1002/anie.200802453.
41. Pathan RA, Bhandari U. Preparation and characterization of the embelin-phospholipids complex as effective drug delivery tool. J Incl Phenom Macrocycl Chem. 2011;69:139–47. https://doi.org/10.1007/s10847-010-9824-2.
42. Singh RP, Gangadharappa HV, Mruthunjaya K. Phospholipids: unique carriers for drug delivery systems. J Drug Deliv Sci Technol. 2017;39:166–79. https://doi.org/10.1016/j.jddst.2017.03.027.
43. Cullis PR, De Kruijff B. Lipid polymorphism and the functional roles of lipids in biological membranes. Biochim Biophys Acta. 1979;559:399–420. https://doi.org/10.1016/0304-4157(79)90012-1.
44. Yang R, Zhang X, Li F. Role of phospholipids and copolymers in enhancing stability and controlling degradation of intravenous lipid emulsions. Colloid Surf A Physicochem Eng Asp. 2013;436:434–42. https://doi.org/10.1016/j.colsurfa.2013.07.022.
45. Hou Z, Li Y, Huang Y, Zhou C, Lin J, Wang Y, et al. Phytosomes loaded with mitomycin C-soybean phosphatidylcholine complex developed for drug delivery. Mol Pharm. 2013;10:90–101. https://doi.org/10.1021/mp300489p.
46. Cai X, Luan Y, Jiang Y, Song A, Shao W, Li Z, et al. Huperzine A-phospholipid complex-loaded biodegradable thermosensitive polymer gel for controlled drug release. Int J Pharm. 2012;433:102–11. https://doi.org/10.1016/j.ijpharm.2012.05.009.
47. Zhang J, Tang Q, Xu X, Li N. Development and evaluation of a novel phytosome-loaded chitosan microsphere system for curcumin delivery. Int J Pharm. 2013;448:168–74. https://doi.org/10.1016/j.ijpharm.2013.03.021.
48. Telange DR, Nirgulkar SB, Umekar MJ, Patil AT, Pethe AM, Bali NR. Enhanced transdermal permeation and anti-inflammatory potential of phospholipids complex-loaded matrix film of umbelliferone: formulation development, physicochemical and functional characterization. Eur J Pharm Sci. 2019;131:23–38. https://doi.org/10.1016/j.ejps.2019.02.006.
49. Singh D, Rawat M, Semalty A, Semalty M. Rutin-phospholipid complex: an innovative technique in novel drug delivery system-NDDS. Curr Drug Deliv. 2012;9:305–14.
50. Singh D, Rawat MSM, Semalty A, Semalty M. Chrysophanol–phospholipid complex. J Therm Anal Calorim. 2012;111:2069–77. https://doi.org/10.1007/s10973-012-2448-6.
51. Jin C, Zhang Z, Xia H, Hu, Jia X. A novel phospholipid complex enriched with micelles: preparation and evaluation in vitro and in vivo. Int J Nanomedicine. 2013:545. https://doi.org/10.2147/ijn.s39526.
52. Tan Q, Liu S, Chen X, Wu M, Wang H, Yin H, et al. Design and evaluation of a novel evodiamine-phospholipid complex for improved oral bioavailability. AAPS PharmSciTech. 2012;13:534–47. https://doi.org/10.1208/s12249-012-9772-9.
53. Alam S, Panda JJ, Chauhan VS. Novel dipeptide nanoparticles for effective curcumin delivery. Int J Nanomedicine. 2012;7:4207–22. https://doi.org/10.2147/IJN.S33015.
54. Shadab MD, Khan RA, Mustafa G, Chuttani K, Baboota S, Sahni JK, et al. Bromocriptine loaded chitosan nanoparticles intended for a direct nose to brain delivery: pharmacodynamic, pharmacokinetic and scintigraphy study in mice model. Eur J Pharm Sci. 2013;48:393–405. https://doi.org/10.1016/j.ejps.2012.12.007.
55. Telange DR, Wavare KD, Patil AT, Umekar MJ, Anand S, Dave VS. Drug-phospholipid complex-loaded matrix film formulation for enhanced transdermal delivery of quercetin. J Excipients Food Chem. 2018;9(2):31–50.
56. Dave V, Telange D, Denge R, Patil A, Umekar M, Gupta SV. Pentaerythritol as an excipient/solid-dispersion carrier for improved solubility and permeability of ursodeoxycholic acid. J Excipients Food Chem. 2018;9:80–95.
57. Telange DR, Bhagat SB, Patil AT, Umekar MJ, Pethe AM, Raut NA, et al. Glucosamine HCL-based solid dispersions to enhance the biopharmaceutical properties of acyclovir. J Excipients Food Chem. 2019;10:65–81.
58. Maiti K, Mukherjee K, Murugan V, Saha BP, Mukherjee PK. Exploring the effect of hesperetin-HSPC complex-a novel drug delivery system on the in vitro release, therapeutic efficacy and pharmacokinetics. AAPS PharmSciTech. 2009;10:943–50. https://doi.org/10.1208/s12249-009-9282-6.
59. Dixit P, Jain DK, Dumbwani J. Standardization of an ex vivo method for determination of intestinal permeability of drugs using everted rat intestine apparatus. J Pharmacol Toxicol Methods. 2012;65:13–7. https://doi.org/10.1016/j.vascn.2011.11.001.
60. Hamilton KL, Butt AG. Glucose transport into everted sacs of the small intestine of mice. Adv Physiol Educ. 2013;37:415–26. https://doi.org/10.1152/advan.00017.2013.
61. Bhattacharyya S, Ahmmed SM, Saha BP, Mukherjee PK. Soya phospholipids complex of mangiferin enhances its hepatoprotectivity by improving its bioavailability and pharmacokinetics. J Sci Food Agric. 2014;94:1380–8. https://doi.org/10.1002/jsfa.6422.
62. Reitman S, Frankel S. A colorimetric method for the determination of serum glutamic oxalacetic and glutamic pyruvic transaminases. Am J Clin Pathol. 1957;28(1):56–63.
63. Kind PR, King EJ. Estimation of plasma phosphatase by determination of hydrolyzed phenol with amino-antipyrine. J Clin Pathol. 1954;7:322–6. https://doi.org/10.1136/jcp.7.4.322.
64. Malloy HT, Evelyn KA. The determination of bilirubin with the photoelectric colorimeter. J Biol Chem. 1937;119:481–90.
65. Ellman GL. Tissue sulfhydryl groups. Arch Biochem Biophys. 1959;82:70–7.
66. Marklund S, Marklund G. Involvement of the superoxide anion radical in the autoxidation of pyrogallol and a convenient assay for superoxide dismutase. Eur J Biochem. 1974;47:469–74. https://doi.org/10.1111/j.1432-1033.1974.tb03714.x.
67. Stocks J, Dormandy TL. The autoxidation of human red cell lipids induced by hydrogen peroxide. Br J Haematol. 1971;20:95–111. https://doi.org/10.1111/j.1365-2141.1971.tb00790.x.
68. Beers RF, Sizer IW. A spectrophotometric method for measuring the breakdown of hydrogen peroxide by catalase. J Biol Chem. 1952;195(1):133–40.
69. Chen ZP, Sun J, Chen HX, Xiao YY, Liu D, Chen J, et al. Comparative pharmacokinetics and bioavailability studies of quercetin, kaempferol and isorhamnetin after oral administration of Ginkgo biloba extracts, Ginkgo biloba extract phospholipid complexes and Ginkgo biloba extract solid dispersions in rats. Fitoterapia. 2010;81:1045–52. https://doi.org/10.1016/j.fitote.2010.06.028.
70. Zhang Q, Sun X, Peng Q, Shi S, Gong T, Zhang J. Preparation, characterization, and in vivo evaluation of a self-nano emulsifying drug delivery system (SNEDDS) loaded with morin-phospholipid complex. Int J Nanomedicine. 2011;3405. https://doi.org/10.2147/ijn.s25824.
71. Semalty A, Semalty M, Singh D, Rawat MSM. Development and physicochemical evaluation of pharmacosomes of diclofenac. Acta Pharma. 2009;59:335–44. https://doi.org/10.2478/v10007-009-0023-x.
72. Saoji SD, Belgamvar VS, Dharashivkar SS, Rode AA, Mack C, Dave VS. The study of the influence of formulation and process variables on the functional attributes of simvastatin-phospholipids complex. J Pharm Innov. 2016;11:264–78. https://doi.org/10.1007/s12247-016-9256-7.

73. Lefevre ME, Olivo R, Vanderhoff JW, Joel ADD. Accumulation of latex in Peyer's patches and its subsequent appearance in villi and mesenteric lymph nodes. Proc Soc Exp Biol Med. 1978;159:298–302.
74. Savić R, Luo L, Eisenberg A, Maysinger D. Micellar nanocontainers distribute to defined cytoplasmic organelles. Science. 2003;300:615–8. https://doi.org/10.1126/science.1078192.
75. Mazumdar A, Dwivedi A, Du Preez JL, du Plessis J. In vitro wound healing and cytotoxic effects of sinigrin - phytosomes complex. Int J Pharm. 2016;498:283–93. https://doi.org/10.1016/j.ijpharm..2015.12027.
76. Pate K, Safier P. Chemical metrology methods for CMP quality. Adv Chem Mech Planazn. 2016;299–325. https://doi.org/10.1016/B978-0-08-100165-3.00012-7.
77. Howard MD, Lu X, Jay M, Dziubla TD. Optimization of the lyophilization process for long-term stability of solid lipid nanoparticles. Drug Dev Ind Pharm. 2012;38(10):1270–9. https://doi.org/10.3109/03639045.2011.645835.
78. Kamiya S, Nozawa Y, Miyagishima A, Kurita T, Sadzuka Y, Sonobe T. Physical characteristics of freeze-dried griseofulvin lipids nanoparticles. Chem Pharm Bull. 2006;54:181–4. https://doi.org/10.1248/cpb.54.181.
79. Ohshima H, Miyagishima A, Kurita T, Makino Y, Wao Y, Sonobe T. Freeze-dried nifedipine-lipid nanoparticles with long-term nano-dispersion stability after reconstitution. Int J Pharm. 2009;377:180–4. https://doi.org/10.1016/j.ijpharm.2009.05.004.
80. Rampino A, Borgogna M, Blasi P, Bellich B, Cesaro A. Chitosan nanoparticles: preparation, size evolution and stability. Int J Pharm. 2013;455:219–28. https://doi.org/10.1016/j.ijpharm.2013.07.034.
81. Crowe LM, Reid DS, Crowe JH. Is trehalose special for preserving dry biomaterials? Biophys J. 1996;71:2087–93. https://doi.org/10.1016/S0006*3495(96)79407-9.
82. Franks F. Freeze-drying of bi-products: putting principles into practice. Eur J Pharm Biopharm. 1998;45:221–9. https://doi.org/10.1016/S0939-6411(98)00004-6.
83. Izutsu KI, Fujimaki Y, Kuwabara A, Aoyagi N. Effect of counterions on the physical properties of I-arginine in frozen solutions and freeze-dried solids. Int J Pharm. 2005;301:161–9. https://doi.org/10.1016/j.ijpharm.2005.05.019.
84. Ruan J, Liu J, Zhu D, Gong T, Yang F, Hao X, et al. Preparation and evaluation of self-nano emulsified drug delivery systems (SNEDDSs) of matrine based on a drug-phospholipid complex technique. Int J Pharm. 2010;386:282–90. https://doi.org/10.1016/j.ijpharm.2009.11.026.
85. Venema FR, Weringa WD. The interactions of phospholipid vesicles with some anti-inflammatory agents. J Colloid Interface Sci. 1988;125(2):484–92.
86. Lasonder E, Weringa WD. An NMR and DSC study of the interaction of phospholipid vesicles with some anti-inflammatory agents. J Colloid Interface Sci. 1990;139:469–78. https://doi.org/10.1016/0021-9797(90)90119-9.
87. Dhore PW, Dave VS, Saoji SD, Bobde YS, Mack C, Raut NA. Enhancement of aqueous solubility and permeability of poorly water-soluble drug ritonavir via lyophilized milk-based solid dispersions. Pharm Dev Technol. 2017;22(1):90–102. https://doi.org/10.1080/10837450.2016.1193193.
88. Zhang WJ, Yang M, Zhu WF, Yue PF, Cai PL, Yuan HL, et al. Process optimization, characterization and pharmacokinetic evaluation in rats of ursodeoxycholic acid-phospholipids complex. AAPS PharmSciTech. 2008;9:322–9. https://doi.org/10.1208/s12249-088-9040-1.
89. Hara H, Ise Y, Morimota N, Shimazawa M, Ichihashi K, Ohyama M, et al. Laxative effects of agawood leaves and its mechanism. Biosci Biotechnol Biochem. 2008;72(2):335–45. https://doi.org/10.1271/bbb.70361.
90. Sharma S, Roy RR, Shrivastava B. Antiproliferative effect of phytosome complex of methanolic extract of terminalia arjuna bark on human breast cancer cell lines (MCF-7). Int J Drug Dev Res. 2015;7(1):173–82.
91. van der Merwe JD, Joubert E, Manley M, de Beer D, Malherbe CJ, Gelderblom WCA. Mangiferin glucuronidation: important hepatic modulation of antioxidant activity. Food Chem Toxicol. 2012;50:808–15. https://doi.org/10.1016/j.fct.2011.11.018.
92. Perrut M, Jung J, Leboeuf F. Enhancement of dissolution rate of poorly soluble active ingredients by supercritical fluid processes. Int J Pharm. 2004;288:3–10. https://doi.org/10.1016/j.ijpharm.2004.09.007.
93. Costa P, Manuel J, Lobô S. Modeling, and comparison of dissolution profiles. Eur J Pharm Sci. 2001;13:123–33.
94. Nicolson GL. The fluid—mosaic model of membrane structure: still relevant to understanding the structure, function, and dynamics of biological membranes after more than 40 years. Biochim Biophys Acta. 2014;1838(6):1451–66. https://doi.org/10.1016/j.bbamem.2013.10.019.
95. Soma CE, Dubernet C, Barratt G, Benita S, Couvreur P. Investigation of the role of macrophages on the cytotoxicity of doxorubicin and doxorubicin-loaded nanoparticles on M5076 cells in vitro. J Control Release. 2008;68(2):283–9. https://doi.org/10.1016/s0168-3659(00)00269-8.
96. Partlow KC, Lanza GM, Wickline SA. Exploiting lipid raft transport with membrane-targeted nanoparticles: a strategy for cytosolic drug delivery. Biomaterials. 2008;29(23):3367–75. https://doi.org/10.1016/j.biomaterials.2008.04.030.
97. Xiong XB, Huang Y, Lu WL, Zhang X, Zhang H, Nagai T. Enhanced intracellular delivery and improved antitumor efficacy of doxorubicin by sterically stabilized liposomes modified with a synthetic RGD mimetic. J Control Release. 2005;107(2):262–75. https://doi.org/10.1016/j.jconrel.2005.03.030.
98. Guo Y, Terazzi E, Seemann R, Fleury RB, Baulin VA. Direct proof of spontaneous translocation of lipid covering hydrophobic nanoparticles through a phospholipids bilayer. Sci Adv. 2016;2(11):1–10. https://doi.org/10.1126/sciadv.1600261.
99. Contini C, Schneemilch M, Gaisford S, Quirke N. Nanoparticle-membrane interactions. J Exp Nanosci. 2018;13(1):62–81. https://doi.org/10.1080/17458080.2017.1413253.
100. Recknagel RO, Glende EA, Dolak JA, Waller RL. Mechanisms of carbon tetrachloride toxicity. Pharmacol Ther. 1989;43:139–54. https://doi.org/10.1016/0163-7258(89)90050-8.
101. Glende EA, Hruszewycz AM, Recknagel RO. Critical role of lipid peroxidation in carbon tetrachloride-induced loss of aminopyrine demethylase, cytochrome P-450, and glucose-6-phosphatase. Biochem Pharmacol. 1976;25:2163–70. https://doi.org/10.1016/0006-2952(76)90128-3.
102. Kim HJ, Bruckner JV, Dallas CE, Gallo GM. Effects of dosing vehicles on the pharmacokinetics of orally administered carbon tetrachlorides in rats. Toxicol Appl Pharmacol. 1990;102:50–60. https://doi.org/10.1016/0041-008x(90)90082-6.
103. Valles EG, De Castro CR, De Castro JA. N-Acetylcysteine is an early but also a late preventive agent against carbon tetrachloride-induced liver necrosis. Toxicol Lett. 1994;71:87–95. https://doi.org/10.1016/0378-4274(94)90202-x.